The histone chaperone activity of SPT2 controls chromatin structure and function in Metazoa

Giulia Saredi[1], Francesco N. Carelli[2,12], Giulia Furlan[2,3,12,13], Stephane Rolland[4,12], Sandra Piquet[5,12], Alex Appert[2,12], Luis Sanchez-Pulido[6], Jonathan L. Price[2,3], Pablo Alcon[7], Lisa Lampersberger[2,3], Anne-Cécile Déclais[8], Navin B. Ramakrishna[2,3,9], Rachel Toth[1], Chris P. Ponting[6], Sophie E. Polo[5], Eric A. Miska[2,3,10], Julie Ahringer[2], Anton Gartner[4,11] and John Rouse[1]

[1]MRC Protein Phosphorylation and Ubiquitylation Unit and [8]Nucleic Acids Structure Research Group, School of Life Sciences, University of Dundee, Dundee DD1 5EH, Scotland, UK; [2]Gurdon Institute, Tennis Court Road, University of Cambridge, Cambridge CB2 1QN, UK; [3]Department of Biochemistry, Tennis Court Road, University of Cambridge, Cambridge CB2 1QW, UK; [4]IBS Center for Genomic Integrity at Ulsan National Institute of Science and Technology (UNIST), Eonyang-eup, Ulju-gun 689-798 (Zipcode 44919), Ulsan, Republic of South Korea; [5]Laboratory of Epigenome Integrity, Epigenetics & Cell Fate Centre, UMR 7216 CNRS - Université Paris Cité, 35 rue Hélène Brion, 75205 Paris Cedex 13, France; [6]MRC Human Genetics Unit, Institute of Genetics and Cancer, University of Edinburgh, Edinburgh EH4 2XU, UK; [7]MRC Laboratory of Molecular Biology, Francis Crick Avenue, Cambridge CB2 0QH, UK; [9]Genome Institute of Singapore (GIS), Agency for Science, Technology and Research (A*STAR), 60 Biopolis Street, Genome, Singapore 138672, Republic of Singapore; [10]Wellcome Sanger Institute, Wellcome Genome Campus, Cambridge CB10 1SA, UK; [11]Department of Biological Sciences, Ulsan National Institute of Science and Technology (UNIST), Eonyang-eup, Ulju-gun, Ulsan 689-798, Republic of South Korea.

[12]These authors contributed equally: Francesco N. Carelli, Giulia Furlan, Stephane Rolland, Sandra Piquet, Alex Appert.

[13]Present address: Transine Therapeutics, Babraham Hall, Cambridge CB22 3AT, UK

Keywords: histone; chaperone; H3.3; nucleosome; chromatin; *C. elegans*; SPT2

Email**:** j.rouse@dundee.ac.uk; g.saredi@dundee.ac.uk

Abstract

Histone chaperones control nucleosome density and chromatin structure. In yeast, the H3-H4 chaperone Spt2 controls histone deposition at active genes but its roles in metazoan chromatin structure and organismal physiology are not known. Here we identify the *Caenorhabditis elegans* orthologue of SPT2 (CeSPT-2) and show that its ability to bind histones H3-H4 is important for germline development and transgenerational epigenetic gene silencing, and that *spt-2* mutants display signatures of a global stress response. Genome-wide profiling showed that CeSPT-2 binds to a range of highly expressed genes, and we find that *spt*-2 mutants have increased chromatin accessibility at these loci. We also show that human SPT2 controls the incorporation of new H3.3 into chromatin. Our work reveals roles for SPT2 in controlling chromatin structure and function in Metazoa.

Introduction

Genomic DNA is packaged into chromatin with the help of histone proteins. The basic units of chromatin are nucleosomes, consisting of 146 bp of DNA wrapped around a histone octamer. The octamer comprises a core histone H3-H4 tetramer flanked by two histone H2A-H2B dimers[1]. The density of nucleosomes in any given region of the genome controls the accessibility of genomic DNA to proteins involved in DNA replication, transcription and DNA repair; local nucleosome density must be altered to facilitate these key processes and restored afterwards[2-4]. A range of proteins in cell nuclei control nucleosome density and composition, including histone chaperones, nucleosome remodelling complexes, histone readers, and histone-modifying enzymes.

Histone chaperones are a structurally diverse class of proteins that bind histones and regulate nucleosome assembly and composition through a variety of mechanisms. These include shuttling of histones between cytoplasm and nucleoplasm, modulating histone stability, and facilitating histone eviction and deposition within nucleosomes[5,6]. Histone chaperones are usually specific for either histones H3-H4, or histone H2A-H2B, and sometimes display specificity for histone variants and their association can be regulated by histone post-translational modifications (PTMs)[5-7]. From a structural perspective, histone chaperone binding shields functional histone interfaces, such as histone-DNA interaction surfaces and histone dimerization domains, that are otherwise engaged when histones are assembled into nucleosomes[5]. Because of their central role in histone metabolism, histone chaperones play crucial roles in DNA replication, transcription and DNA repair[3,5,8].

Transcription has a major impact on chromatin structure, especially as the progression of the RNA polymerase II (RNAPII) complex disrupts nucleosomes when it encounters them in the DNA template, leading to "unpeeling" of DNA from the histone octamer[9-11]. Cryo-EM studies revealed that, upon engaging with a nucleosome, RNAPII complexes stall at specific locations along the "unpeeled" nucleosomal DNA[11,12]. During this process, the histone surfaces bound by nucleosomal DNA are transiently exposed and recognised by histone chaperones[13-15]. For example, the histone chaperones SPT6, SPT5, ASF1 and the HIRA and FACT chaperone complexes have been implicated in promoting histone disassembly and recycling at active genes[8,16-19]. Conditional depletion of yeast FACT subunits or Spt6 leads to a transcription-dependent loss of H3-H4 from genes, mis-localisation of parental histone PTMs, and compensatory increase in new histone

35   deposition over gene bodies[17,20]. Similarly, impaired binding of yeast Spt5 to histone H3-H4

36   leads to reduced nucleosome occupancy at active genes, loss of H3K4 trimethylation from

37   transcription start sites (TSS) and lethality[16]. Active genes are enriched for the histone

38   replacement variant H3.3[21-23]. Histone H3.3-H4 deposition during transcription is mediated

39   by the HIRA complex[21,22,24], which is composed of three subunits: HIRA, UBN1 and

40   CABIN1. HIRA promotes both the incorporation of new H3.3-H4 as well as the recycling of

41   parental H3.3-H4[18], in a manner that specifically requires HIRA interaction with the UBN1 or

42   ASF1 histone chaperones[18], respectively. Therefore, the preservation of chromatin

43   structure and nucleosome density during transcription requires multiple histone chaperones

44   with overlapping but non-equivalent functions.

45

46   Budding yeast Spt2 is a poorly understood histone chaperone implicated in histone H3-H4

47   recycling during transcription[25,26]. Spt2 (also called Sin1) was identified genetically:

48   mutations in the *SPT2* gene suppress transcriptional initiation defects associated with

49   transposon insertions in the *HIS4* gene promoter[27] or mutations in the Swi/Snf or SAGA

50   chromatin remodelling complexes[28]. Further work revealed that Spt2 associates with the

51   protein-coding regions of highly expressed genes, in a manner that requires Spt6[26,29].

52   Moreover, loss of Spt2 results in decreased association of H3 with these regions[26]. Yeast

53   Spt2 was shown to bind to cruciform DNA *in vitro*[30], which is thought to reflect an affinity for

54   crossed DNA helices, reminiscent of DNA at the entry-exit of a nucleosome[31]. Yeast cells

55   lacking Spt2 show an increase in spurious transcription from cryptic intragenic start

56   sites[26,27], and Spt2 mutations in the H3-H4 binding domain recapitulate these defects[25].

57   Furthermore, Spt2 cooperates with the yeast Hir (HIRA) complex in suppressing spurious

58   transcription[26]. Therefore, Spt2 plays an important role in regulating H3-H4 recycling and

59   chromatin structure in yeast. Little is known, however, about the roles and regulation of

60   SPT2 beyond budding yeast. Chicken (*Gallus gallus*) *SPT2* is a non-essential gene, the

61   product of which is found in both the nucleoplasm and nucleoli[32]. Chicken SPT2 interacts

62   with RNA polymerase I (RNAPI) and was reported to support RNAPI-mediated

63   transcription, as measured *in vitro* by nuclear run-on assay[32]. Both the DNA binding and

64   histone binding regions of chicken SPT2 are necessary to support this function[32]. Even

65   though almost nothing is known about SPT2 function in human cells, an X-ray crystal

66   structure of the histone binding domain (HBD) of human SPT2 bound to a H3-H4 tetramer

67   has been reported[25]. This analysis revealed two alpha helices (αC1 and αC2) and a

4

68 connecting loop which all make contact with the tetrameric form of H3-H4. Mutating

69 conserved residues in αC2, or mutating Met641 located in the inter-helical loop, reduced

70 SPT2 binding to H3-H4 *in vitro*[25]. Replacing the HBD in yeast Spt2 with the human HBD

71 suppresses cryptic transcription, similar to wild type yeast Spt2, but mutating Met641 in the

72 chimeric protein blocks this suppression[25]. These data suggest that human SPT2 can

73 regulate H3-H4 function, at least in yeast, but similar roles in human cells have not yet been

74 described.

75

76 In this study, we dissect the *in vivo* function of SPT2 using the model organism *C. elegans*.

77 We combine structural modelling, biochemistry and genetics approaches to characterise

78 how SPT2 binding to histone H3-H4 regulates chromatin structure and function in Metazoa,

79 and we show that worm SPT2 regulates chromatin density at highly expressed genes,

80 transgenerational epigenetic silencing, and animal fertility upon heat stress. We also

81 provide evidence that SPT2 regulates chromatin assembly in human cells.

82

Results

Identification of a *C. elegans* orthologue of the SPT2 histone chaperone

We set out to test if SPT2 histone binding activity is relevant for chromatin structure and function in Metazoa. The nematode *C. elegans* has proven a valuable system to investigate the role of chromatin modulators at the cell and organism level[33-38], and we decided to interrogate a role for SPT2 in this organism first. However, no *C. elegans* orthologue of SPT2 had been reported when we started this project. Iterative similarity searches revealed the uncharacterized open reading frame *T05A12.3* as a putative orthologue. Multiple sequence alignments defined three evolutionarily conserved regions of the T05A12.3 protein product. The first region spans residues 1-129 (red box) and is conserved in metazoan orthologues but not in budding yeast (Fig. 1a). The second region spans residues 250-276 (yellow box) and is conserved from yeast to humans. The functions of these domains are unknown. The third region, spanning residues 572 to 661, is the region of highest conservation and corresponds to the histone binding domain (HBD) found in the human and yeast Spt2 orthologues[25] (Fig. 1a, purple box; Fig. S1a). We used the crystal structure of the human SPT2 HBD[25] as a search template to generate a structural homology model for the corresponding region of T05A12.3, which revealed three points of similarity between the two proteins. First, the tertiary structure of the putative T05A12.3 HBD adopts an arrangement that is strikingly similar to the human HBD: αC1 and αC2 helices connected by a loop (Fig. 1b). Second, both helices and the loop contact H3-H4 in our model, and the residues involved are conserved. For example, Glu637 and Glu638 in the worm T05A12.3 HDB correspond to Glu651 and Glu652 in the αC2 helix of the human HBD known to be required for H3-H4 binding[25]. Also, Met627 in the T05A12.3 HBD contacts H4 in our model; Met627 is the equivalent of Met641 in the human protein which contacts H4 and contributes to H3-H4 binding[25] (Fig. 1c, Fig. S1b). Third, the most highly conserved residues in each of the two helices and loop lie at the interface with H3-H4 (Fig. 1c). Therefore, structural modelling strongly suggests that worm T05A12.3 is a H3-H4 binding orthologue of SPT2, and we refer to T05A12.3 hereafter as CeSPT-2.

We next tested if CeSPT-2 binds to histone H3-H4 *in vitro*. To this end we purified His$_6$-tagged, full-length recombinant CeSPT-2 and human (Hs) SPT2 (Fig. 1d) and performed a pull-down experiment using recombinant histone H3-H4 complex covalently coupled to beads. As shown in Fig. 1e, CeSPT-2 binds histone H3-H4 *in vitro* similar to HsSPT2, and the isolated putative HBD of CeSPT2 also bound to H3-H4 (Fig. 1f, WT HBD). We next

6

117 tested the effect of substituting Met627, the equivalent of Met641 which contacts H4 in the

118 H3-H4 tetramer[25] (Fig. 1c, Fig. S1b). Substituting Met627 for Ala (M627A) in the isolated

119 CeSPT2 HBD reduced, but did not abolish, binding to immobilized H3-H4, similar to the

120 M641A substitution in the HsSPT2 HBD analysed in parallel (Fig. 1f). Similar results were

121 obtained using purified full-length CeSPT-2 (Fig. 1g-i). We also found that CeSPT-2 binds

122 to synthetic cruciform DNA (Fig. S1c), similar to HsSPT2[32] and that the CeSPT2 M627A

123 substitution had no apparent effect on cruciform DNA binding (Fig. S1d). Hereafter, we refer

124 to the histone binding-defective mutation encoding the CeSPT-2 M627A substitution as

125 "HBM".

126

127 We expected CeSPT-2 to be a nuclear protein given that it binds H3-H4 and DNA. Analysis

128 of a worm strain in which GFP was inserted at the 5′ end of the *T05A12.3* gene showed that

129 GFP-tagged CeSPT-2 is a widely expressed protein found, for example, in the head,

130 germline, hypodermis, intestine and vulva cell nuclei (Fig. S1e, upper row). Moreover,

131 knock-in of the HBM mutation did not affect GFP::CeSPT-2 expression or localisation (Fig.

132 S1e, lower row). Taken together, the data above indicate that CeSPT-2 is a widely

133 expressed, nuclear protein which appears to be the orthologue of the SPT2 histone H3-H4

134 chaperone.

135

Loss of CeSPT-2 histone binding activity causes germline defects and temperature-dependent sterility

138 In order to study the impact of CeSPT-2 on worm development and fertility, two

139 independently derived *spt-2* null strains, with the open reading frame being eliminated, were

140 constructed, hereafter referred to as *spt-2*[KO-A] and *spt-2*[KO-B] (Fig. 2a). The *spt-2* null strains

141 were viable, and their progeny size was comparable to wild type under standard growth

142 conditions (20°C, Fig S2a). However, when worms were grown at 25°C for one generation,

143 we noticed that a low proportion of worms produced far fewer progeny than wild type (Fig.

144 2b; Table S1). We next investigated if this apparent fertility defect became more

145 pronounced in subsequent generations (Fig. 2c). As shown in Fig. 2d and e, the proportion

146 of sterile *spt-2* null worms increased progressively with each generation, so that after 10

147 generations at 25°C very few or no fertile worms remained. We also generated a knock-in

148 worm strain harbouring the HBM mutation that reduces CeSPT-2 binding to H3-H4 (*spt-2*[HBM]) (Fig. 2a). The *spt-2*[HBM] worms also showed an increased incidence of sterility when

150 grown at 25°C for several generations, although to a lesser extent than the *spt-2* null strains

151 (Fig. 2e, Fig. S2b) probably because the CeSPT-2 HBM shows residual binding to H3-H4

152 (Fig. 1f, h). To be certain that the sterility observed in the *spt-2*[HBM] strain is a direct

153 consequence of M627A mutation, we reverted the Ala627 HBM mutation to wild type

154 (Met627). The resulting strain (*spt-2*[HBM] A627M) lost the sterility phenotype associated with

155 *spt-2*[HBM] indicating that the sterility is due to loss of CeSPT-2 histone binding capacity (Fig.

156 S2b).

157

158 To investigate the morphology of the germline in *spt-2*-defective worms, we grew *spt-2*[KO-B]

159 worms for several generations at 25°C and subjected the siblings of worms that showed a

160 reduced number of progeny or sterility to microscopic analysis (Fig. S2c, d). In wild type

161 nematode gonads, germ cells transit in an orderly manner from the mitotic stem cell state to

162 the various stages of meiotic prophase (pachythene and diplotene) and eventually become

163 fully mature oocytes (diakinesis stage)[39] (Fig. 2f). In contrast, the germlines of *spt-2* null

164 worms whose siblings had a decreased progeny size show a wide array of defects at 25°C

165 (generations G4 and G5, Fig. S2d), including: i) a low number of fertilized embryos, which

166 appeared rounded and incapable of hatching or further development (Fig. 2g); ii) oocytes

167 but no productive fertilization, and presenting an abrupt transition between pachytene cells

168 and oocytes (Fig. 2h); iii) a highly distorted germline showing mis-localization of oocytes

169 (Fig. 2i); and iv) signs of masculinization, as evidenced by an excessive number of sperm

170 cells (Fig. 2j). The germlines of siblings of worms that were completely sterile were reduced

171 in volume, contained a small number of enlarged mitotic germ cells, and showed

172 vacuolization (Fig. 2k, S2e). Taken together these data show that the onset of sterility in

173 *spt-2* defective worms is associated with pleiotropic defects in germ line development.

174

175 **CeSPT-2 histone binding activity is required for transgenerational maintenance of**

176 **nuclear RNAi-mediated gene silencing**

177 The sterility seen in *spt-2* defective worms after several generations at elevated

178 temperature was reminiscent of worms harbouring defects in nuclear RNA interference

179 (RNAi)[40,41]. Nuclear RNAi is a pathway in which small double-stranded (ds) RNAs trigger

180 heritable gene silencing[42,43]. The establishment of silencing involves dsRNA-mediated

181 dicing of the target mRNA, while the maintenance and transgenerational inheritance of the

182 silenced state involves the RNA-dependent synthesis of secondary siRNAs and changes in

183 chromatin state in the RNAi target gene(s), such as histone H3 methylation at Lys9 and

184 Lys23[44-47]. In prevailing models, the Argonaute family protein HRDE-1 binds secondary

185 small RNAs and is required for the transgenerational inheritance of gene silencing after the

186 dsRNA trigger has been removed. HRDE-1 directs H3K9 trimethylation at RNAi target loci,

187 although how chromatin promotes the inheritance of gene silencing across several

188 generations is poorly understood[48].

189

190 We investigated a role for CeSPT-2 in the nuclear RNAi pathway, using a reporter strain we

191 described previously[42]. In this system, a *gfp::h2b* single-copy transgene which is

192 constitutively expressed in the worm germline can be silenced by feeding worms with

193 bacteria expressing double-stranded *gfp* RNA (*gfp* RNAi)[42] (Fig. 3a). Analysis of GFP

194 fluorescence showed that silencing of the *gfp::h2b* reporter transgene occurs normally in

195 *spt-2* null and *hrde-1*-defective worms grown on bacteria expressing the *gfp* RNAi (P0)

196 (Figs. 3b, c). After removing the bacteria, silencing was maintained for 5 generations in the

197 wild type worms, but the transgene was de-silenced in the first generation (G1) of *hrde-1*-

198 defective worms. Strikingly, the reporter transgene was robustly de-silenced in both of the

199 *spt-2* null strains from the second generation (G2) after the removal of the *gfp* RNAi, as

200 measured by GFP fluorescence (Fig. 3b, c) and mRNA abundance (qPCR) (Fig. 3d). We

201 also found that the *spt-2*[HBM] strain showed transgene de-silencing albeit slightly later than in

202 the null strains (Figs. 3e, f). Taken together, these data show that CeSPT-2 histone binding

203 activity is required for the transgenerational inheritance of epigenetic gene silencing.

204

205 **CeSPT-2 binds and controls the chromatin structure of highly transcribed genes**

206 To gain insight into the endogenous genes that might be regulated by CeSPT-2, we sought

207 to identify its chromatin occupancy genome-wide. We performed chromatin

208 immunoprecipitation and sequencing (ChIP-seq) in synchronized adult worms expressing

209 endogenously tagged GFP::CeSPT-2, using wild type worms as control. Around 88% of the

210 genomic CeSPT-2 target sites we identified lie within genic regions (5299/6003 sites), with

211 the remaining sites found in intergenic (~7%, 258 sites) or repetitive (~4%, 446 sites)

212 sequences (Fig. 4a). GFP::CeSPT-2 associates over the entire length of what we hereby

213 call as 'CeSPT-2 target genes', with an apparent enrichment for the 3' end of the gene (Fig.

214 4b). We reasoned that a histone chaperone with a potential function during transcription

215 would associate with genes in a transcription-dependent manner. Indeed, CeSPT-2 bound

9

216   genes are highly expressed, and their transcriptional levels are positively correlated with

217   CeSPT-2 chromatin binding (Fig. 4c).

218

219   We next asked whether loss of CeSPT-2 – or loss of its histone H3-H4 binding activity –

220   affects chromatin accessibility of the genes it is enriched at. We performed ATAC-seq in

221   wild type, *spt-2*KO-A and *spt-2*HBM adult worms and found that chromatin accessibility

222   increased across the entire length of the gene body of CeSPT-2 bound genes (Fig. 4d, e,

223   Fig. S3a). In contrast, no significant increase in chromatin accessibility was observed at

224   genomic regions that are not enriched for CeSPT-2 (Fig. S3b). Notably, most genes

225   showing a significant increase in their accessibility in *spt-2* mutants had high levels of

226   CeSPT-2 binding (Fig. 4f). Therefore, CeSPT-2 binds and influence the chromatin

227   architecture of some of the most highly transcribed genes in *C. elegans*.

228

229   We next sought to evaluate a potential role for CeSPT-2 on gene expression. The

230   expression of most CeSPT-2 bound genes did not change significantly in *spt-2* null worms

231   compared with wild type (Fig. 4g), with only 1.8% (40/2177) and 0.18% (4/2177)

232   targets showing a marked up- or downregulation in the mutant, respectively (FDR<0.001

233   and log2 fold change >1 or <-1; Supplementary Table 2). While we might have expected

234   more accessible chromatin to result in increased gene expression, CeSPT-2 bound genes

235   are among the most highly expressed genes in adult worms (Fig. 4c) and we speculate that

236   a further increases in the expression of these genes may not be possible. While CeSPT-2

237   target gene expression appeared to be unaffected in *spt-2* null worms, global mRNA-seq

238   analysis of CeSPT-2 non-target genes revealed a pronounced up-regulation of gene

239   expression in these worms compared with wild type (Fig. 4h). Specifically, we found 40

240   protein-coding genes downregulated and 605 genes upregulated in *spt-2* null worms

241   (FDR<0.001 and log$_2$ fold change >1 or <-1; Fig. S3c: validation by qPCR using

242   independently harvested RNA). Of the 605 up-regulated genes, only 40 were CeSPT-2

243   targets. The up-regulated genes were strongly enriched Gene Ontology (GO) terms related

244   to 'defense response', 'protein dimerization' and 'nucleosome' (Fig. 4i, S3d), indicating that

245   *spt-2* KO worms experience activation of a global stress response. The HBM mutants

246   showed a similar increased expression of 'defense response' genes (Fig. 4i), although gene

247   up-regulation was less dramatic in *spt-2*HBM worms; around 80% of the genes up-regulated

248   in *spt-2*HBM worms are also up-regulated in the *spt-2*KO strain. Taken together, these data

249   show that CeSPT-2 binds to a range of highly expressed target genes, and its histone

250 binding activity controls chromatin accessibility at these loci; loss of *spt-2* results in a global

251 stress response.

252

SPT2 controls new histone H3.3 levels and deposition in human cells

254 The data above show clear roles for CeSPT-2 activity in controlling chromatin maintenance

255 in worms, and we explored a potential role in human cells. We first tested if HsSPT2

256 associates with chromatin. Affinity-purified antibodies raised against HsSPT2 recognised a

257 band of approximately 75 kDa in extracts of U-2-OS cells, that was reduced in intensity by

258 three different HsSPT2-specific siRNAs (Fig. S4a). Fractionation experiments showed that

259 endogenous HsSPT2 is strongly enriched in the chromatin fraction of U-2-OS cells (Fig.

260 5a). Furthermore, fluorescence analysis of U-2-OS cells after pre-extraction of soluble

261 proteins showed clearly that HsSPT2 tagged with GFP at either the N-terminus or C-

262 terminus associates with chromatin (Fig. 5b). An HsSPT2 deletion fragment (aa 1-570)

263 lacking the HBD bound chromatin similar to full-length HsSPT2, indicating that interaction

264 with H3-H4 does not mediate chromatin association (Fig. 5b, S4b, c). Consistent with this

265 idea, a deletion fragment corresponding to the HBD alone (aa 571-end) localized to the

266 nucleus but was not retained on chromatin (Fig. 5b, S4b, c).

267

268 We next tested if HsSPT2 influences histone H3.3 deposition, which is enriched at active

269 genes[22]. With this goal in mind, we employed a reporter cell line stably expressing a SNAP-

270 tagged H3.3[49] which can be covalently labelled *in vivo* using cell-permeable compounds to

271 distinguish between pre-existing and newly synthetised protein pools. To specifically

272 visualise newly incorporated H3.3, we used a quench-chase-pulse approach: we first

273 labelled all pre-existing H3.3-SNAP with the non-fluorescent chemical bromothenylpteridine

274 (BTP, quench), we allowed a 2-hour chase period to synthesize new histones, and we

275 finally labelled new H3.3-SNAP with the fluorophore tetramethylrhodamine (TMR, pulse;

276 Fig. 5c). To analyse the total levels of new H3.3-SNAP (which are a measure of H3.3

277 synthesis and stability), we fixed cells and measured H3.3-SNAP-TMR intensity in cell

278 nuclei (Fig. 5c). Furthermore, to assess the incorporation of newly synthesised H3.3 into

279 chromatin, we pre-extracted soluble proteins prior to fixing the cells and then measured

280 TMR fluorescence intensity (Fig. 5c). As shown in Fig. 5d and e, siRNA-mediated depletion

281 of HsSPT2 reduces both the total levels of SNAP-tagged new H3.3 (direct fixation, Fig. 5d)

282 as well as the amount of new H3.3 incorporated into chromatin (pre-extraction, Fig. 5e).

283 New H3.3 incorporation is reduced after depletion of HIRA (Fig. 5e), as previously

11

284 shown[18,22]. We note that H3.3-SNAP mRNA levels in HsSPT2-depleted cells are

285 comparable to control cells (Fig. S4d). Moreover, HsSPT2 knock-down does not affect

286 HIRA stability, nor does it impair HIRA binding to chromatin (Fig. S4e, f). From these data,

287 we conclude that human SPT2 controls histone H3.3 levels and promotes their

288 incorporation into chromatin.

289

290 **Functional interplay between the SPT-2 and HIRA-1 histone chaperones in *C. elegans***

291 Given the roles for SPT2 and HIRA in new H3.3 deposition in human cells, we queried

292 whether CeSPT-2 and HIRA-1 may overlap functionally in worms. *hira-1* null worm strains

293 are known to be viable but show pleiotropic defects, including low brood size and

294 morphological defects (such as small pale bodies and protruding vulvas "Pvl")[36,37]. We set

295 out to test the impact of the concomitant loss of CeSPT-2 and HIRA-1 on worm

296 development and viability. With this in mind, we depleted HIRA-1 by RNAi from wild type,

297 *spt-2* null or *spt-2*HBM worms grown at 25°C. We noted that the Pvl phenotype, reported in

298 *hira-1* null worms[37], was not observed in wild type worms treated with *hira-1* RNAi (Fig. 5f),

299 possibly due to partial HIRA-1 depletion. However, HIRA-1 depletion in *spt-2* null or *spt-*

300 *2*HBM worms resulted in a dramatic increase in the incidence of vulvar protrusions and of

301 burst nematodes (Fig. 5f). The morphological defects of the *spt-2*HBM were fully rescued in

302 the reverted (A627M) strain (Fig. 5f). Comparison of the transcriptomes of *spt-2* null (this

303 study) and *hira-1* null worms (dataset from ref.[36]) revealed a statistically significant overlap

304 of the genes up-regulated in both mutants, the up-regulated genes being enriched for stress

305 response transcripts (Fig. 5g). From these data, we conclude that the CeSPT-2 and HIRA-1

306 histone chaperones have overlapping functions in the control of H3-H4 deposition in worms,

307 and that HIRA-1 becomes essential for worm fitness in *spt-2* mutants.

308

12

Discussion

309 In this study we presented the first demonstration that SPT2 controls chromatin structure

310 and function in Metazoa. Through bioinformatic analyses and structural modelling we

311 identified the previously unannotated protein T05A12.3 as the worm orthologue of CeSPT-2

312 (Fig. 1a-c), and we found that recombinant CeSPT-2 binds H3-H4 *in vitro* in a manner

313 similar to the yeast and human orthologues (Fig. 1d-i). Global profiling revealed that

314 CeSPT-2 targets a range of genomic sites in worms, the vast majority (~88%) lying within

315 genic regions (Fig. 4a, b). Consistent with what has been observed in yeast[26], genes

316 enriched for CeSPT-2 are amongst the mostly highly active genes in worms (Fig. 4c),

317 possibly reflecting a propensity of CeSPT-2 to bind accessible chromatin regions. CeSPT-2

318 target genes showed increased chromatin accessibility over the entire bodies of these

319 genes in *spt-2* null and *spt-2*[HBM] worms (Fig. 4d, e), with a direct correlation between

320 CeSPT-2 binding levels and extent of increased accessibility (Fig. 4f); therefore CeSPT-2

321 activity helps preserve the integrity of chromatin in actively transcribed regions.

322

323 Intriguingly, the expression of most CeSPT-2 target genes was unaffected in the *spt-2* null

324 and *spt-2*[HBM] worms (Fig. 4g). However, as CeSPT-2-bound genes are among the most

325 highly expressed in worms, it may be that their expression is already maximal in wild type

326 worms. What, then, is the role of CeSPT-2 in limiting chromatin accessibility at these

327 genes? Perhaps CeSPT-2 activity prevents harmful consequences of an excessively open

328 chromatin such as spurious transcription, as observed for yeast Spt2. This might lead to the

329 production of aberrant transcripts resembling foreign nucleic acids[50] or neo-antigens. A

330 wide range of stress response genes were upregulated in *spt-2* mutant worms (Fig. 4h, i),

331 and it is tempting to speculate this protective response is triggered by aberrant transcripts.

332 This possibility will be interesting to investigate.

333

334 The idea that CeSPT-2 binding to H3-H4 preserves chromatin integrity at highly expressed

335 genes is supported by our demonstration that RNAi-mediated transgenerational gene

336 silencing of a *gfp::h2b* reporter transgene requires CeSPT-2 histone binding activity (Fig.

337 3a-f). This finding, to our knowledge, identifies CeSPT-2 as the first histone chaperone

338 required for nuclear RNAi in *C. elegans*. How chromatin structure controls the

339 transgenerational inheritance of *gfp::h2b* silencing is unclear: while histone PTMs

340 associated with silenced chromatin are observed at the RNAi target locus in response to

341 dsRNA[44-47,51], the SET-25 and SET-32 H3K9/K23 tri-methyltransferases are only required

343 for maintenance of silencing in the first generation after removal of the dsRNA trigger, and

344 dispensable afterwards[44,52]. We speculate that CeSPT-2 is recruited to the open chromatin

345 of the active transgene, and controls silencing of the *gfp::h2b* reporter by limiting chromatin

346 accessibility, as shown for the endogenous CeSPT-2 target genes above (Fig. 4d, f). It will

347 be interesting in the future to test if loss of CeSPT-2 influences the repressive H3 PTMs

348 associated with RNAi-mediated gene silencing, as well as whether other histone

349 chaperones are required for transgenerational gene silencing.

350

351 We do not yet know how SPT2 is targeted to chromatin. The C-terminal HBD is the most

352 highly conserved region of SPT2, but at least in human cells it is not required for

353 association with chromatin (Fig. 5b). However, one of the other two conserved regions we

354 identified in our bioinformatic analyses (Fig. 1a) may promote SPT2 binding to chromatin,

355 either directly or through an as yet unidentified binding partner. We note that our sequence

356 conservation analysis was unable to confirm the presence of a previously described HMG-

357 box domain (InterPro: IPR009071) in SPT2[53], which was suggested to mediate DNA

358 binding. Examination of the SPT2 AlphaFold models also failed to reveal an L-shape

359 arrangement of three α-helices, which is characteristic of the HMG-box domain[54]. In yeast,

360 the first 200 amino acids of Spt2 are necessary and sufficient for Spt2 recruitment to active

361 genes, and for association with Spt6 which recruits Spt2 to target genes[29]. Whether

362 metazoan SPT2 binds to SPT6 (and other components of the active RNA polymerase II

363 complex) is not known, and mechanism behind SPT2 recruitment to chromatin in Metazoa

364 remain to be elucidated.

365

366 Besides SPT2, the histone chaperones FACT, SPT6, SPT5, ASF1, and HIRA have all been

367 implicated in maintaining chromatin structure at active genes[17,18,20]. One possible scenario

368 to explain the multiplicity of chaperones acting at transcribed genes is that SPT2 could work

369 together with the other histone chaperones, potentially in a partially redundant manner, by

370 binding different configurations of histone H3-H4 during nucleosome assembly and

371 disassembly. Histone turnover is highest at the most highly expressed genes[55-58], and these

372 genes may be particularly reliant on the joint functions of CeSPT-2 together with other

373 histone chaperones. In this light, we found that RNAi depletion of HIRA-1 causes profound

374 defects in *spt-2* null or *spt-2*[HBM] mutant worms, but not in wild type worms (Fig. 5f),

375 indicating that H3-H4 binding by CeSPT-2 likely supports a step of chromatin assembly that

376 becomes essential in the absence of HIRA-1.

14

377

378   Our data from human cells shows that HsSPT2 depletion decreases the total levels of new

379   H3.3 as well as the levels of chromatin-bound new H3.3 (Fig. 5c-e), suggesting that SPT2

380   can also function in regulating the production and/or stability of soluble histones. We cannot

381   exclude that the decreased incorporation of H3.3-SNAP is simply a by-product of

382   decreased H3.3 stability although we note, for example, that mutations in histone H3 that

383   impair binding to the MCM2 histone chaperone affect total levels of SNAP-tagged H3.1

384   without decreasing new H3.1 incorporation[59]. SPT2 was recently identified as an interactor

385   of the histone chaperone and heat shock folding chaperone DNAJC9[60]; investigating a

386   potential interplay between SPT2 and folding chaperones in promoting histone stabilisation

387   during transcription will be of great interest.

388

389   Faithful maintenance of chromatin structure is essential to safeguard epigenetic information

390   and cell identity, and to preserve genome stability and organism viability. Our research

391   presents the first detailed *in vivo* characterisation of metazoan SPT2 histone chaperone

392   function. We show the importance of CeSPT-2 in maintaining germline fertility under heat

393   stress conditions, and its role in preserving chromatin structure at highly active genes and

394   ensuring the transgenerational inheritance of gene silencing. Together, our work highlights

395   the importance of understanding how the concerted action of histone chaperones come

396   together to preserve chromatin structure and organism fitness.
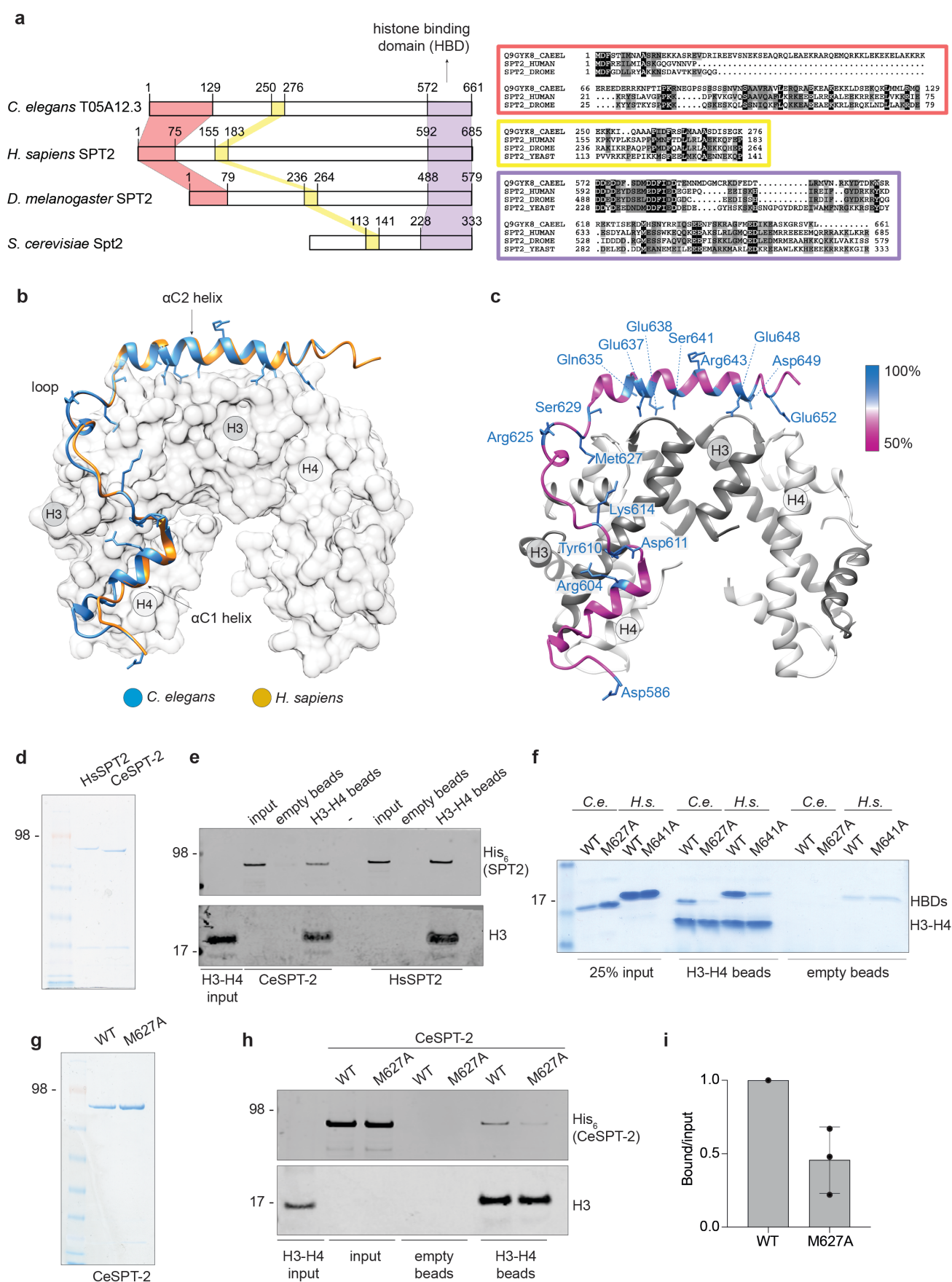
397

Figure 1

Figure 1. Identification of the *C. elegans* orthologue of SPT2

a, Schematic representation of the three evolutionarily conserved regions found in SPT2 orthologues and in *C. elegans T05A12.3* (left panels). N-terminal, central and C-terminal (HBD) regions are shown shaded in red, yellow, and violet, respectively. Multiple sequence alignments corresponding to the three conserved regions are shown inside coloured boxes in red, yellow, and violet, respectively (right panels). The amino acid colouring scheme indicates the average BLOSUM62 score (correlated to amino acid conservation) in each alignment column: black (greater than 3.5), grey (between 3.5 and 1.5) and light grey (between 1.5 and 0.5). Sequences are named according to their UniProt identifier. Species abbreviations: Q9GYK8_CAEEL, *Caenorhabditis elegans*; SPT2_HUMAN, *Homo sapiens*; SPT2_DROME, *Drosophila melanogaster*; SPT2_YEAST; *Saccharomyces cerevisiae.* **b**, Structural homology model for the putative HBD of *C. elegans* T05A12.3 (blue). This was generated using the crystal structure of the *H. sapiens* SPT2 HBD (yellow) in complex with the H3-H4 tetramer (shaded white) as a search template (PDB code 5BS7[25]). The positions of the αC1 and αC2 helices and the connecting loop are shown. **c**, Same as d, except that only the CeSPT-2 HBD is shown, colour-coded according to the degree of amino acid conservation. **d**, Coomassie gel staining of recombinant full-length HsSPT2 and CeSPT-2 produced in bacteria. **e**, Pull-down of full-length recombinant CeSPT-2 or human HsSPT2 with beads covalently coupled to histone H3-H4 in the presence of 500mM NaCl. One representative experiment of two is shown. **f**, H3-H4 pull-down with recombinant CeSPT-2 HBD (wild type (WT) or histone binding mutant (M627A)), or HsSPT-2 HBD (wild type (WT) or histone binding mutant (M641A)). One representative experiment of three is shown. **g**, Coomassie gel staining of recombinant full-length CeSPT-2 (WT and M627A). **h**, H3-H4 pull-down with full-length recombinant CeSPT-2 WT and M627A. **i**, Quantification of the three independent replicates of the H3-H4 pull-downs. n=3; data are represented as mean ± S.D.
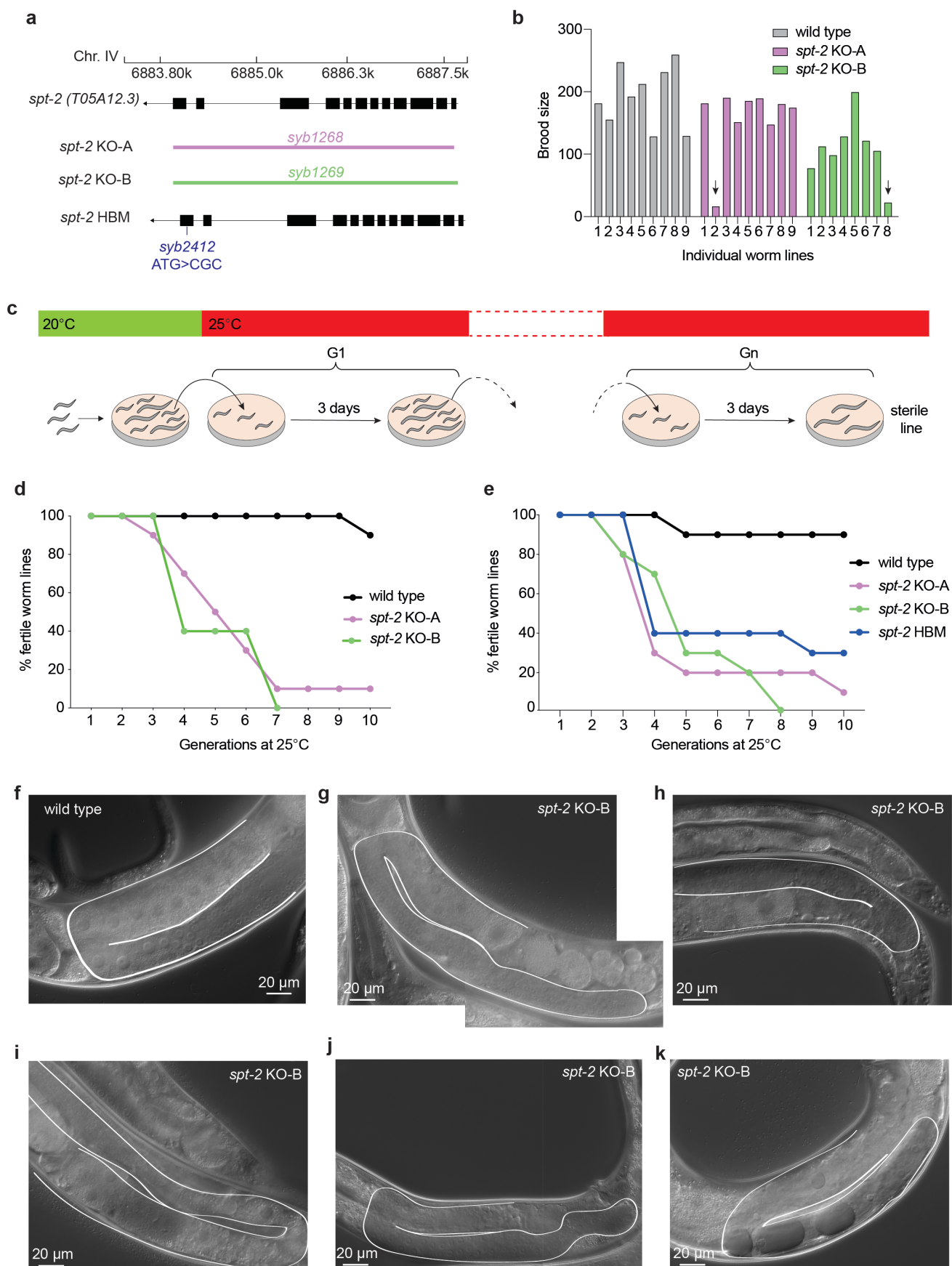
17

Figure 2

429 **Figure 2. Loss of CeSPT-2 histone binding causes germline defects and sterility**

430 **a**, Schematic diagram of the wild type, *spt-2*KO and *spt-2*HBM alleles. The genomic location of

431 the *spt-2* (*T05A12.3*) gene on chromosome IV is shown. Coloured bars indicate the deleted

432 regions in the *spt-2* gene in the knockout strains. **b**, The brood size of worms from the

433 indicated strains, grown at 25°C from the L4 stage, is shown. Arrows indicate worms with

434 low brood size. The number of worms used is indicated in the figure. **c-e**, Transgenerational

435 sterility assay. Three L4 stage worms of the indicated genotypes were shifted to 25°C and

436 grown at that temperature for the indicated number of generations. Every generation (3

437 days), three L3-L4 worms were moved to a new plate. A worm line was considered sterile

438 when no progeny was found on the plate. Ten plates per genotype were used, n=10. **f-k**.

439 Single wild type and *spt-2*KO-B L4 worms were shifted to 25°C and grown at that temperature

440 for the indicated number of generations; every generation (3 days), one L4 worm was

441 moved to a new plate and the number of progeny was assessed, as indicated in Fig. S2d.

442 Siblings of the worms that, three days after the L4 stage, showed reduced or no progeny

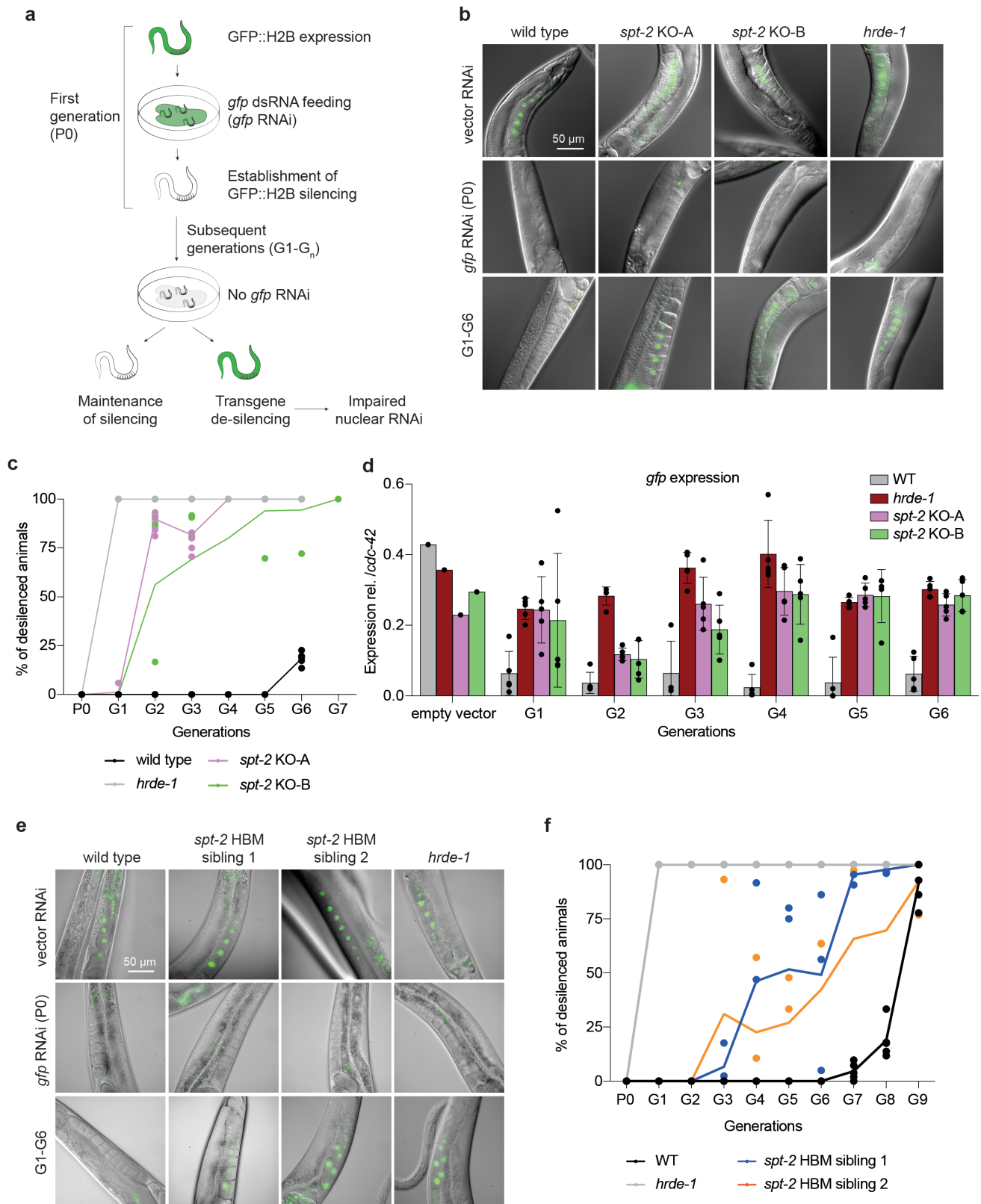443 were subjected to microscopic observation one day after the L4 stage.

444

Figure 3

445
446

447 **Figure 3. CeSPT-2 histone binding is required for transgenerational gene silencing**

448 **a**, Schematic diagram of the transgenerational RNAi assay described previously[42]. **b**,

449 Representative images of the germline of the *gfp::h2b* reporter worm strains without RNAi

450 (vector RNAi), after *gfp::h2b* RNAi treatment and in the subsequent generations after

451 removal of the dsRNA (G1-G6). **c**, Quantification of GFP::H2B expression. Worms showing

452 "dim" GFP intensity during microscopy inspection were considered as silenced. The graph

453 indicates the mean percentage of de-silenced worm lines across the replicate lines (mean ±

454 S.D.), and the percentage of de-silenced worms in each replicate is indicated by a dot; n=5.

455 **d**, *gfp::h2b* mRNA expression measured by qPCR, normalized relative to *cdc-42*. n=1 for

456 'empty vector' point; n=5 for G1-G6; data are represented as mean ± S.D. **e**,

457 Representative microscopy images of the germline of the indicated worm strains without

458 RNAi (vector RNAi), after *gfp::h2b* RNAi treatment and in the subsequent generations after

459 removal of the dsRNA (G1-G9). **f**, Quantification of GFP::H2B expression, as in c. The

460 graph indicates the mean percentage of de-silenced worm lines across the replicate lines

461 (mean ± S.D.), and the percentage of de-silenced worms in each replicate is indicated by a

462 dot; n=5 (WT and *hrde-1* mutant); n=3 (for each of the *spt-2*[HBM] siblings).

463
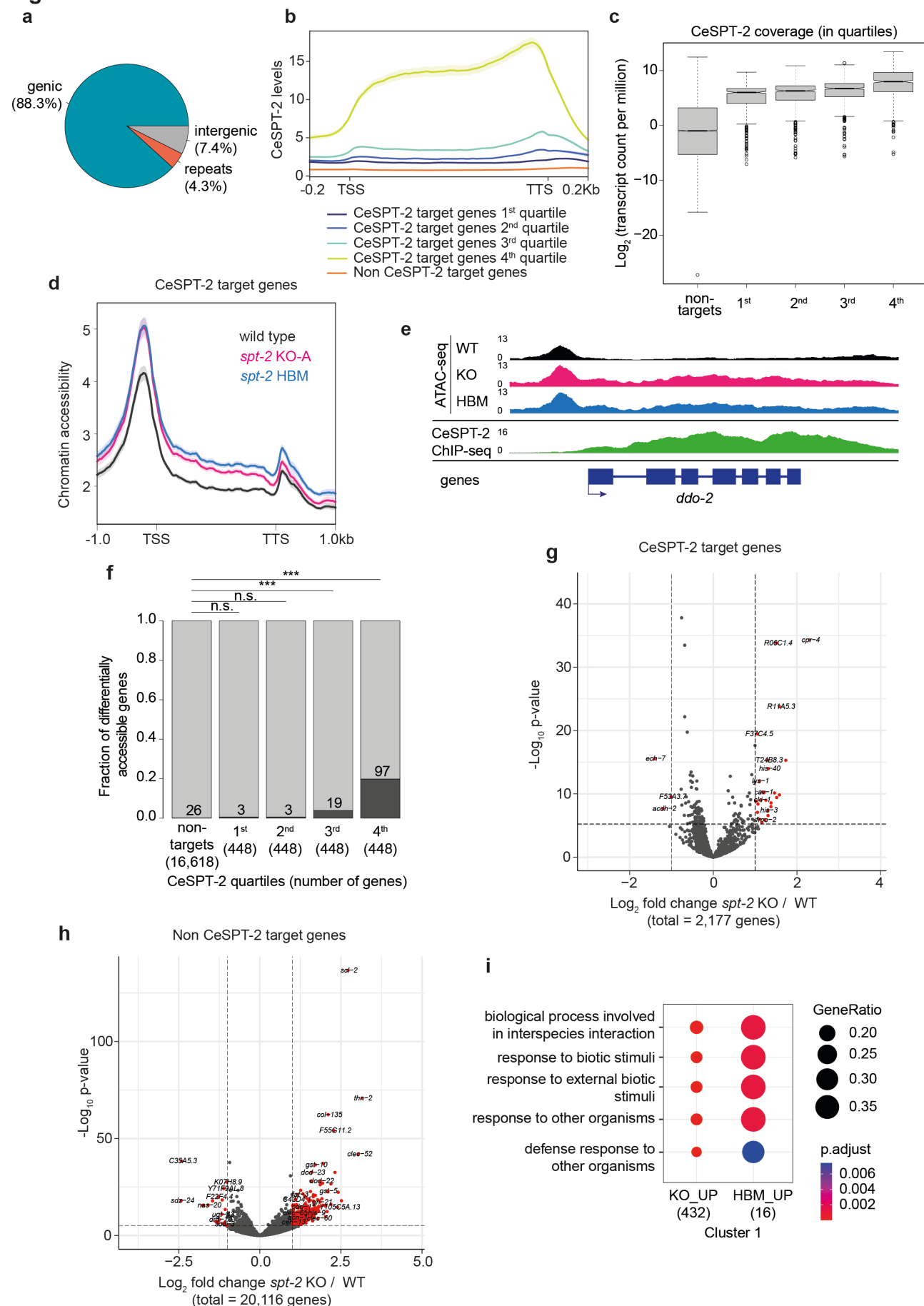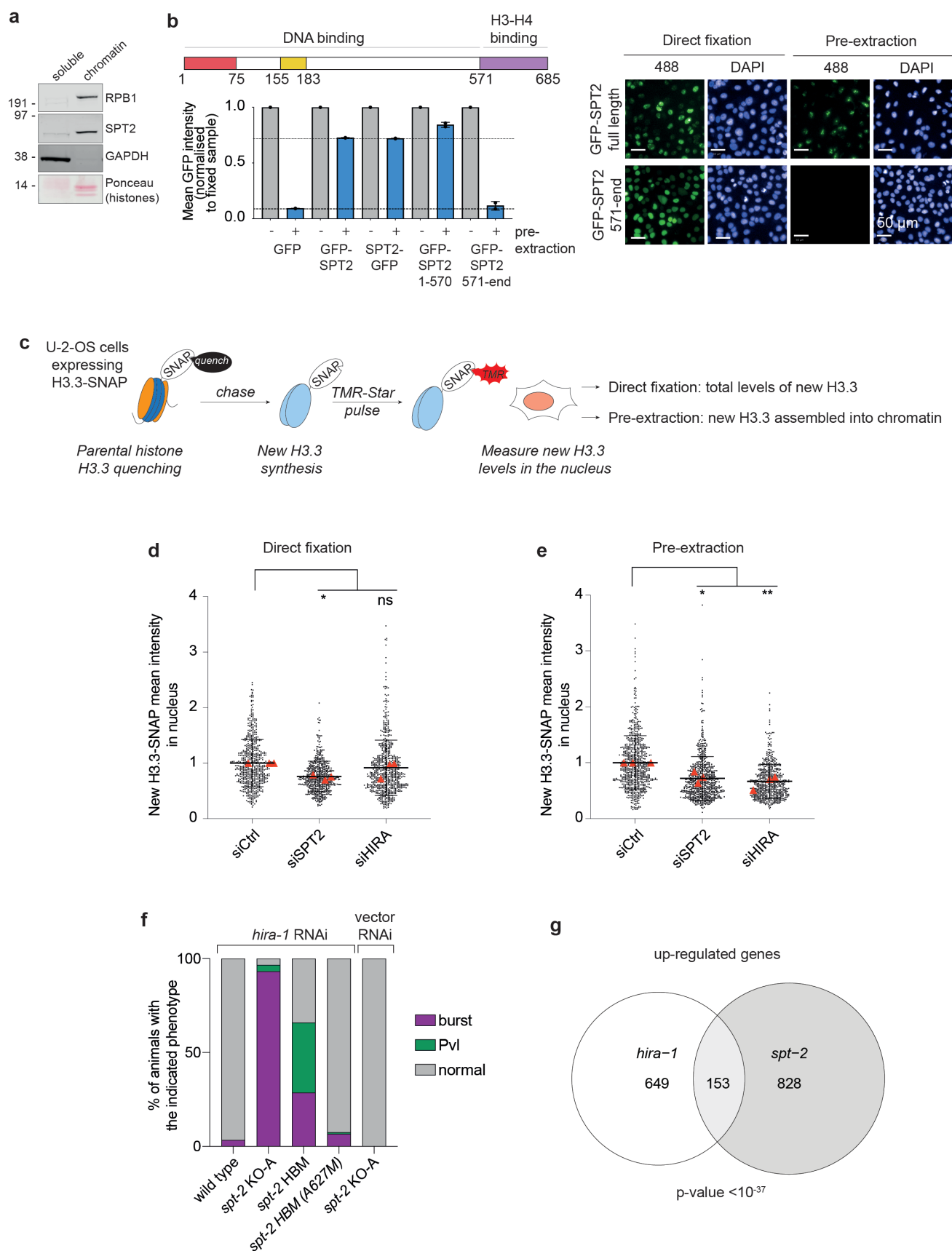
Figure 4

464

465 **Figure 4. CeSPT-2 histone binding controls chromatin accessibility**

466 **a,** Distribution of GFP::CeSPT-2 ChIP-seq peaks in different genome locations. **b**,

467 Metagene profile of GFP::CeSPT-2 occupancy levels within the coding region of its target

468 genes, compared to non CeSPT-2 target genes. **c**, GFP::CeSPT-2 chromatin occupancy

469 regions were divided in quartiles, and gene expression levels (measured in synchronised

470 wild type adult worms) were plotted in each quartile, and compared to CeSPT-2 non-target

471 genes. The box represents the interquartile range, the whiskers the min and max (excluding

472 outliers). **d**, Chromatin accessibility at CeSPT-2 target genes in *spt-2*$^{KO-A}$ and *spt-2*^{HBM} adult

473 worms, measured by ATAC-seq and expressed in reads per million. TSS, transcription start

474 site; TTS, transcription termination site. Two independent replicates of the ATAC-seq

475 experiment were performed. **e**, Example of ATAC-seq and GFP::CeSPT-2 ChIP-seq tracks.

476 The ATAC-seq signal across the gene body of *ddo-2* in wild type, *spt-2*$^{KO-A}$ and *spt-2*^{HBM}

477 worms is indicated, with the GFP::CeSPT-2 binding profile shown in the bottom profile. **f**,

478 Fraction of genes with significantly increased accessibility in *spt-2*$^{KO-A}$ (dark grey) among

479 CeSPT-2 non-target and target genes. CeSPT-2 targets were divided in quartiles based on

480 their CeSPT-2 enrichment. Statistical difference between CeSPT-2 targets and non-targets

481 was measured by a chi-squared test. Benjamini-Hochberg corrected p values: n.s.: p >

482 0.05; ***: p < 0.001. **g, h**, Volcano plot of gene expression levels of CeSPT-2 target genes

483 (g) and non-targets (h) in *spt-2* null versus wild type worms. Red points indicate genes with

484 FDR<0.001 and log$_2$ fold change >1 or <-1. **i**, Gene Ontology (GO) analysis of the genes

485 upregulated in the indicated *spt-2* mutants.

486

23

Figure 5

487
488

489   **Figure 5. SPT2 is required for histone H3.3-H4 deposition in human cells**

490   **a**, Distribution of HsSPT2 between soluble and chromatin fractions of U-2-OS cells. **b**, GFP-

491   HsSPT2 binding to chromatin in fixed or pre-extracted U-2-OS cells assessed by high-

492   content microscopy. Graph shows the mean GFP intensity normalised to the fixed sample;

493   n=2, data are represented as mean with range of two independent experiments. **c**,

494   Schematics of the SNAP-tag assay for new histone H3.3 incorporation. **d, e**, Fluorescence

495   intensity of TMR-labelled SNAP-H3.3 in U-2-OS SNAP-H3.3 cell nuclei after (d) direct

496   fixation or (e) pre-extraction. Cells were harvested 48 hours post siRNA transfection. Data

497   are represented as mean ± S.D. from 3 independent experiments (red triangles) and

498   normalized to the mean of siCtrl in the same experiment. **f,** Percentage of burst worms or

499   worms showing a protruding vulva (Pvl) phenotype upon treatment with *hira-1* RNAi, or

500   empty vector RNAi, as indicated. Forty worms were scored per replicate, and three

501   independent replicates of the experiment were performed. **g**, Venn diagram showing the

502   overlap between up-regulated genes in *spt-2* null and *hira-1* null worms. Hypergeometric

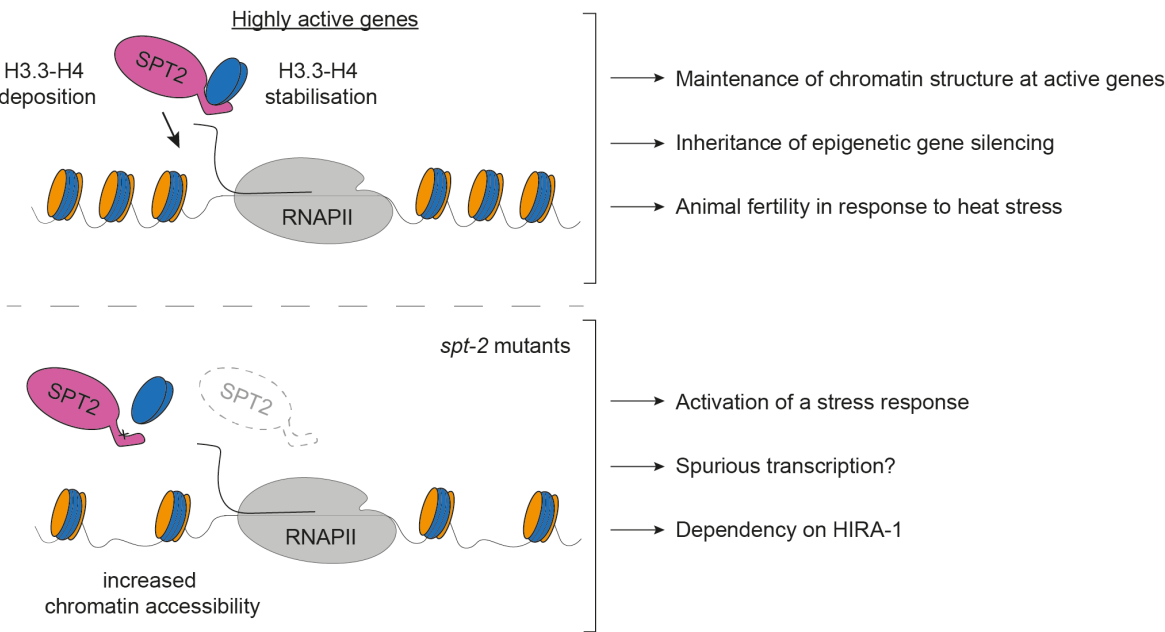503   test; enrichment: 3.085, p value < 10^{-37}.

504

Figure 6

505
506
507

508 **Figure 6. Model**

509 SPT2 localises to highly active genes where it promotes the maintenance of chromatin

510 structure via its histone H3-H4 binding capacity. Here, it may act via stabilising new histone

511 H3.3 prior to their incorporation, as well as via directly promoting their incorporation into

512 chromatin. In worms, the interaction of CeSPT2 with H3-H4 is required for the

513 transgenerational inheritance of gene silencing and to promote the integrity of the germline

514 under heat stress conditions. Loss of *spt-2*, or impaired SPT-2 binding to histones, activates

515 a stress response, potentially due to aberrant transcription, and makes worms reliant on the

516 HIRA-1 H3.3-H4 histone chaperone.

517

Author Contributions

GS and JR conceived the project. FNC analysed ChIP-seq, ATAC-seq and mRNA-seq datasets under the supervision of JA. GF and LL performed the transgenerational gene silencing microscopy assay under the supervision of EAM. SR and AG analysed GFP::SPT-

552   2 distribution and germline defects. SP performed SNAP-H3.3 experiments under the

553   supervision of SEP. AA performed ATAC-seq, and AA and GS performed GFP::SPT-2

554   ChIP-seq. JLP and NBR performed the initial RNA-seq analysis. LS-P and CPP identified

555   the *C. elegans* SPT-2 orthologue. ACD performed EMSA assays. PA performed molecular

556   modelling of CeSPT-2. RT performed the cloning of human expression vectors. GS

557   performed the remaining experiments, and GS and JR wrote the manuscript.

558

559   **Declaration of Interests**

560   The authors declare no competing interests. E.A.M. is a founder and director of STORM

561   Therapeutics Ltd. STORM Therapeutics had no role in the design of the study and

562   collection, analysis, and interpretation of data as well as in writing the manuscript.

563

564   **Data Availability**

565   All plasmids and antibodies generated in this study can be requested to the MRC PPU

566   DSTT: https://mrcppureagents.dundee.ac.uk/reagents-from-papers/Rouse-SPT2-paper-1

567   All NGS datasets have been deposited on GEO with accession number GSE224802.

568   Other materials generated in this work will be made available upon request.

569

570   **Materials and Methods**

571

572   **Computational protein sequence analysis**

573   Multiple sequence alignments were generated with the program T-Coffee using default

574   parameters[61], slightly refined manually and visualized with the Belvu program[62]. Profiles of

575   the SPT2 evolutionarily conserved regions as hidden Markov models (HMMs) were

576   generated using HMMer. Profile-based sequence searches were performed against the

577   Uniref50 protein sequence database[63] using HMMsearch[64,65].

578

579   **Structural modelling and conservation analysis**

580   The crystal structure of human SPT2 (Protein Data Bank [PDB] code 5BS7)[25] was used as

581   a search template to generate a structural homology model for *C. elegans* SPT-2 using the

582   homology-model server SWISS-MODEL (swissmodel.expasy.org)[66,67]. A multiple protein

583   sequence alignment was generated by MUSCLE (ebi.ac.uk/Tools/msa/muscle)[68]. UCSF

584   Chimera[69] was used to align the atomic models of human and *C. elegans* Set using the

585   "MatchMaker" function. Protein sequence conservation was mapped onto the structural

586   model and figures generated in Chimera.

587

588   **Recombinant protein purification**

589   All recombinant SPT2 proteins were expressed in Rosetta 2(DE3)pLysS BL21 *E. coli*

590   bacteria (Novagen, 71401). Plasmids were transformed into Rosetta BL21 cells according

591   to the manufacturer's instructions and transformed bacteria were grown in LB medium

592   supplemented with 35 µg/ml chloramphenicol and 50µg/ml of kanamycin.

593   <u>Full-length CeSPT-2 (wild type and HBM) and HsSPT2 (His$_6$-tagged)</u>

594   Expression of 2xFlag-SUMO-CeSPT-2-His$_6$ or of 2xFlag-SUMO-HsSPT2-His$_6$ was induced

595   by growing bacteria overnight at 20°C with 200µM IPTG. After cell lysis (Lysis buffer: 50mM

596   Tris-HCl pH 8.1, 500mM NaCl, 10mM imidazole pH 8, 10% glycerol, 0.1mM TCEP

597   supplemented with protease inhibitors), lysates were incubated with NiNTA beads for 1

598   hour rotating top-down at 4°C, and subsequently washed with Lysis buffer. Proteins were

599   eluted by addition of 500mM imidazole (Elution buffer: 50mM Tris-HCl pH 8.1, 500mM

600   NaCl, 500mM imidazole pH 8, 10% glycerol, 0.1mM TCEP supplemented with protease

601   inhibitors) and Flag M2 beads were immediately added to the eluate, and incubated for 2

602   hours rotating top-down at 4°C. The M2 beads were washed twice with Lysis buffer

603   supplemented with 10mM $MgCl_2$ and 2mM ATP to remove folding chaperones. Flag-tagged

604   proteins were eluted twice by adding Lysis buffer containing 0.5mg/ml Flag peptide (MRC

605   PPU Reagents and Services). The eluate was incubated with 200nM His_6-Ulp1 (prepared

606   as previously described[70]) rotating top-down for 1 hour at 4°C. The cleaved 2xFlag-SUMO

607   tag was removed by re-binding the eluate on Flag M2 beads rotating top-down for 1 hour at

608   4°C and collecting the unbound fraction. Proteins were concentrated in an Amicon Ultra

609   Centrifugal tube with a molecular weight cut-off of 30kDa and frozen in liquid nitrogen.

610   <u>CeSPT-2 HBD (aa. 552-661) and HsSPT2 HBD (aa. 571-685) wild type and HBMs</u>

611   Expression of His_{14}-SUMO-CeSPT-2 HBD or His_{14}-SUMO-HsSPT2 HBD was induced by

612   growing bacteria overnight at 20°C with 400µM IPTG. After cell lysis (Lysis buffer: 20mM

613   Tris-HCl pH 7.5, 200mM NaCl, 40mM imidazole pH 8, 0.1mM TCEP supplemented with

614   protease inhibitors), lysates were incubated with NiNTA beads for 2 hours rotating top-down

615   at 4°C and washed with Lysis buffer. Proteins were eluted by addition of 500mM imidazole

616   (Elution buffer: 20mM Tris-HCl pH 7.5, 500mM NaCl, 500mM imidazole pH 8, 0.1mM TCEP

617   supplemented with protease inhibitors). The eluate was incubated with 60µM His_6-Ulp1 to

618   cleave the His_{14}-SUMO tag and dialysed overnight against Dialysis buffer (20mM Tris-HCl

619   pH 7.5, 500mM NaCl, 0.1mM TCEP). The cleaved His_{14}-SUMO tag was removed by re-

620   binding the eluate on NiNTA beads and collecting the unbound fraction containing the SPT2

621   HBD. Proteins were concentrated in a Amicon Ultra Centrifugal tube with molecular weight

622   cut-off of 3kDa and frozen in liquid nitrogen.

623

Histone H3-H4 pull-down

625   Protein LoBind tubes were used at all steps. For each reaction, 10µl of Pierce NHS-

626   activated magnetic beads (ThermoFisher, 88826) were prepared according to the

627   manufacturer's instructions. Briefly, the beads were washed with 1ml of cold 1mM HCl and

628   then were resuspended in 1mL of Coupling Buffer (500mM NaCl, 200mM $NaHCO_3$, pH

629   8.3). 20pmol of recombinant histone H3.1-H4 tetramer (NEB, M2509S) were immediately

630   added to the tube. The reaction was incubated overnight at 4°C with top to bottom rotation.

631   The following day, the beads were washed twice with 0.1M glycine (pH 2.0) and once with

632   MilliQ water. 1mL of Quenching Buffer (500mM ethanolamine, 500mM NaCl pH 8.5) was

633   added to the beads, followed by 2 hours incubation at 4°C. The beads were then washed

634   once with MilliQ and twice with Binding Buffer (20mM Tris-HCl pH 8.0, 500mM NaCl, 0.1%

635   Triton-X100, 0.1mM TCEP). 5pmol of recombinant SPT2 proteins were added to the beads

636   in 800µl Binding Buffer and incubated for 1.5 hours at 4°C, rotating top-down. The beads

637   were then washed 3 times with Washing Buffer (20mM Tris-HCl pH 8.0, 700mM NaCl, 0.1%

638   Triton-X100, 0.1mM TCEP), each time rotating for 15 minutes on a top-down wheel at 4°C.

639   The beads were then boiled for 10 minutes in 1XLDS buffer (supplemented with 150mM

640   DTT) and the supernatant was loaded on a 4-12% NuPage Bis-Tris gel. For the H3-H4 pull-

641   down using the isolated HBD, the protocol was the same as above, except for the following

642   differences: NHS-activated Sepharose 4 Fast Flow beads (Cytiva, 17090601) instead of

643   magnetic beads were used; 1nmol of recombinant *Xenopus laevis* H3(Δ1-40 aa.)-H4 (a gift

644   from Ramasubramanian Sundaramoorthy and Tom Owen-Hughes) and 0.5nmol of

645   recombinant CeSPT-2 or HsSPT2 HBDs were used; the eluted material was run on a

646   home-made 18% acrylamide gel and then stained with InstantBlue (Abcam) Coomassie

647   protein staining.

648

649   **Electrophoretic Mobility Shift Assay**

650   <u>Preparation of labelled HJ substrates.</u> An equimolar mixture of all four oligonucleotides

651   (J3b(40), J3h(40), J3r(40) and J3x(40)) was 5'-^{32}P-labelled, then annealed by slow-cooling.

652   The four-way junction was purified by electrophoresis on a native 8% polyacrylamide gel

653   and recovered by the crush and soak method followed by ethanol precipitation. <u>Binding</u>

654   <u>assays.</u> The substrate (10nM) was incubated with increasing amounts of SPT2 at 37°C for

655   15 minutes in binding buffer (25mM Tris-HCl pH 8.0, 55mM NaCl, 1mM EDTA, 1mM DTT,

656   0.1mg/ml BSA, 1% glycerol), then mixed with loading buffer (Ficoll 400, 2.5% final) and

657   run on a native 8% polyacrylamide gel at 8 V/cm for 2 hours. The gel was then dried,

658   exposed to a Storage Phosphor screen, and quantified with a Typhoon FLA 9500

659   phosphorimager (GE Healthcare).

660   Oligonucleotide sequences (5' – 3') are:

661   J3b(40): AGGGATCCGTCCTAGCAAGGGGCTGCTACCGGAAGCTTAC

662   J3h(40): GTAAGCTTCCGGTAGCAGCCTGAGCGGTGGTTGAATTCAC

663   J3r(40): GTGAATTCAACCACCGCTCAACTCAACTGCAGTCTAGAAC

664   J3x(40): GTTCTAGACTGCAGTTGAGTCCTTGCTAGGACGGATCCCT

665

666   **General *C. elegans* maintenance and strains**

667   The list of strains used in this study is provided below. Unless otherwise indicated, worms

668   were grown on 1xNGM media plates (3 g/L NaCl, 2.5 g/L peptone, 20 g/L agar, 5 mg/L

31

669   cholesterol, 1mM CaCl$_2$, 1mM MgSO$_4$, 2.7g/L KH$_2$PO$_4$, 0.89 g/L K$_2$HPO$_4$) seeded with

670   OP50 bacteria. Worms were routinely kept at 20°C. All *spt-2* alleles used in this study were

671   generated by SunyBiotech using the CRISPR-Cas9 technology. All *spt-2* mutant strains

672   were back-crossed 6 times against the reference wild type N2 strain.

673

Analysis of GFP::SPT-2 tissue expression

675   For the analysis of the tissue expression of GFP::SPT-2, L4 animals were mounted in M9

676   buffer with 0.25mM levamisole on 2% agarose pads. Imaging was performed at 20°C using

677   a microscope equipped with a 63X 1.25 NA oil lens (Imager M2; Carl Zeiss, Inc.) and a

678   charge-coupled device camera (Axiocam 503 mono). Nomarski and GFP Z-stacks

679   (2µm/slice) were sequentially acquired using the Zeiss acquisition software (ZEN 3.1 blue

680   edition). The same LED intensity and acquisition time was used for all images (Nomarski

681   (50%, 20ms), GFP (50%, 100ms)).

682

Brood size analysis

684   Worms at the L4 stage were singled onto 1xNGM plates with a thin layer of OP50 bacteria

685   and allowed to grow at either 20°C or 25°C. Worms were passaged to a new plate every

686   12-24 hours to keep generations separated, and fertilised eggs and L1 larvae were counted

687   until each adult was not laying eggs anymore. Worms that were not alive by the end of the

688   experiment were discarded from the analysis.

689

Transgenerational sterility assay

691   Worms of the indicated genotypes were grown at 20°C before shifting to 25°C at the L4

692   stage. Either one or three L4 larvae (as indicated in the figure legend) were placed on each

693   1xNGM plate seeded with OP50 bacteria and grown at 25°C. Every 3 days, three L3-L4

694   larvae were transferred to a new plate. Worms were considered sterile when no progeny

695   was found on the plate. Ten plates per genotype were used in each repetition of the assay.

696

***hira-1* RNA interference**

698   RNAi was performed by feeding worms with HT115 bacteria containing L4440 plasmids that

699   express double-stranded RNA. The plasmid expressing *hira-1* dsRNA was obtained from a

700   commercial RNAi library (clone III-2P01, Source Bioscience), and the empty L4440 vector

701   was used as a control. dsRNA expression was induced by adding IPTG to a final 3mM

702 concentration in LB media supplemented with 50µg/ml ampicillin, and RNAi bacteria were

703 seeded on 1xNGM plates at OD_{600} equal 1. When the plate was dry, six L4 worms of the

704 indicated genotypes were added to the plate and allowed to grow at 25°C until the next

705 generation (2 days). New *hira-1* RNAi, or vector RNAi, plates were prepared as described

706 above. Forty L2-L3 worms per genotype were singled on the RNAi plates and allowed to

707 grow at 25°C for four/five days, after which plates were blindly scored for Pvl phenotype

708 and presence of burst worms.

709

710 **Transgenerational memory inheritance**

711 Three L4 larvae per genotype were plated on *gfp* RNAi-expressing bacteria (5 replicates for

712 each *spt-2*[KO] strain, or 3 replicates for each *spt-2*[HBM] sibling) or empty vector L4440 bacteria

713 (3 replicates). Generation 1 (G1) animals were analysed under a fluorescence microscope,

714 and one silenced animal per replicate per genotype was plated onto HB101 bacteria. At

715 each generation, one silenced animal was singled from each plate to produce the next

716 generation, and the remaining adult progeny was analysed under a Kramer FBS10

717 fluorescence microscope. Animals were collected in M9 buffer, washed twice, quickly fixed

718 in 70% ethanol, and deposited onto a glass slide coated with a 2% agarose pad. At least 35

719 animals per replicate per genotype were counted at each generation. Germline nuclear

720 GFP brightness was scored as 'on' or 'off' by visual inspection (dim GFP expression was

721 scored as 'off'). Representative images were taken on a SP8 confocal fluorescence

722 microscope (Leica) at 40X magnification.

723

724 **GFP::CeSPT-2 chromatin-immunoprecipitation and sequencing**

725 Animals of the indicated genotype (grown at 20°C) were bleached, and embryos allowed to

726 hatch overnight in M9 buffer. Approximately 300,000 worms were used per condition,

727 divided in six 15cm plates seeded with thick HB101 bacteria. Synchronized adult animals

728 (70h post-seeding) were washed 4 times in M9. Worms were flash-frozen in liquid nitrogen

729 to obtain 'popcorns' which were ground using a BioPulverizer (MM400 Mixer Mill, Retsch)

730 liquid nitrogen mill, until adult worms were broken in 3-4 pieces each. Worm powder was

731 resuspended in cold PBS (supplemented with Roche cOmplete protease inhibitors). Freshly

732 prepared EGS solution (ethylene glycol bis(succinimidyl succinate)) was added to a final

733 1.5mM concentration and incubated rotating for 8 minutes, followed by crosslinking with 1%

734 methanol-free formaldehyde (ThermoFisher, 28908) for 8 minutes and quenching with

735 glycine (final concentration 125mM). The crosslinked chromatin was then washed twice in

736 PBS (with protease inhibitors) and once in FA buffer (50mM HEPES/KOH pH 7.5, 1mM

737 EDTA, 1% Triton-X100, 0.1% sodium deoxycholate, 150mM NaCl) supplemented with

738 protease (Roche Complete) and phosphatase (PhosStop) inhibitors. Chromatin was then

739 sonicated using a Bioruptor (Diagenode) on High mode, 30 cycles at 30 sec ON, 30 sec

740 OFF. A 30µl aliquot was de-crosslinked to confirm enrichment of DNA fragments between

741 100bp and 300bp. To de-crosslink, chromatin was spun down at maximum speed and the

742 supernatant was transferred to a new tube and resuspended in FA buffer supplemented

743 with 2µl of 10mg/ml RNase A (incubation at 37°C for 10 minutes) followed by Proteinase K

744 treatment (incubation at 65°C for 1 hour). DNA concentration was measured using the

745 Qubit assay (Qubit dsDNA High Sensitivity assay, ThermoFisher). The ChIP reaction was

746 assembled as follows: 20µg of DNA were used per ChIP reaction, together with 10µg of

747 GFP antibody (ab260) in 1mL of FA buffer (with protease and phosphatase inhibitors)

748 supplemented with 1% sarkosyl. ChIP reactions were incubated overnight rotating at 4°C.

749 For each reaction, 40µl of protein A magnetic beads slurry were blocked overnight in 1mL

750 of FA buffer (with protease and phosphatase inhibitors) supplemented with 10µl of tRNA

751 (Merck, R5636). The following day, beads were added to the IP reaction and incubated for

752 a further 2 hours rotating at 4°C. The beads were then washed with 1ml of the following

753 buffers (ice cold), each time rotating 5 minutes at 4°C: two times with FA buffer (with

754 protease and phosphatase inhibitors); once with FA buffer supplemented to 500mM NaCl;

755 once with FA buffer supplemented to 1M NaCl; once with TEL buffer (10mM Tris-HCl pH 8,

756 250mM LiCl, 1% NP-40, 1% sodium deoxycholate, 1mM EDTA) and finally twice in TE

757 buffer (pH 8). DNA was eluted twice with 60µl of ChIP Elution buffer (1% SDS, 250mM

758 NaCl in TE buffer pH 8), each time incubating for 15 minutes at 65°C (300rpm shaking).

759 Eluted samples were treated with 2µl of 10mg/ml RNase A for 1 hour at 37°C and then de-

760 crosslinked overnight at 65°C with 1.5µl of 20mg/mL Proteinase K. DNA was purified with

761 PCR purification columns and DNA concentration was measured with the Qubit assay.

762 <u>Sequencing library preparation.</u> The library preparation was performed as previously

763 described[71] using a modified Illumina TruSeq protocol. Briefly, DNA fragments were first

764 treated with End repair enzyme mix (NEB, E5060) for 30 min at 20°C in 50µl volume, and

765 DNA fragments were subsequently recovered with one volume of AMPure XP beads

766 (Beckman Coulter, A63880) mixed with one volume of 30% of PEG_{8000} in 1.25M NaCl. DNA

767 was eluted in 17µl of water and further 3' A-tailed using 2.5 units of Klenow 3' to 5' exo(-)

768 (NEB, cat M0212) in 1X NEB buffer 2 supplemented with 0.2 mM dATP for 30 minutes at

769 37°C. Illumina Truseq adaptors were ligated to the DNA fragments by adding 25µl of 2X

770   Quick Ligase buffer (NEB, M2200), 1µl of adaptors (1µl of a 1:250 dilution of Illumina stock

771   solution), 2.5µl water and 1.5 ml of NEB Quick ligase (NEB, M2200). The reaction was

772   incubated 20 minutes at room temperature and 5µl of 0.5M EDTA was added to inactivate

773   the ligase enzyme. DNA was purified using 0.9 volume of AMPure XP beads, and DNA

774   fragments were eluted in 20µl water. 1µl of DNA was used to set up a qPCR reaction to

775   determine the number of cycles needed to get amplification to 50% of the plateau, which is

776   the cycle number that will be used to amplify the library. 1µl of DNA was mixed with 5µl of

777   KAPA Syber Fast 2X PCR master mix and 1µl of 25µM Truseq PCR Primer cocktail. Each

778   library (19µl) was then amplified with 20µl of KAPA HiFi HotStart Ready Mix (KM2605) and

779   subsequently size selected to a size between 250bp and 370bp. To achieve this, DNA was

780   first purified with 0.7 volumes of AMPure beads to remove all fragments above 370bp,

781   keeping the supernatant and discarding the beads. All DNA fragments were then recovered

782   from the supernatant by adding 0.75 volumes of beads and 0.75 volumes of 30% PEG_{8000}

783   in 1.25M NaCl, and eluted in 40µl of water. To recover fragments above 250bp, 0.8

784   volumes of beads were added to bind the library. DNA was then eluted in 10µl of water,

785   quantified using a dsDNA HS Qubit kit, and the size distribution of the libraries was

786   analyzed using an Agilent Tapestation.

787

788   **Processing of sequencing data**

789   ATAC-seq and ChIP-seq reads were pre-processed using trim-galore (version 0.6.7;

790   available at https://github.com/FelixKrueger/TrimGalore) and mapped on the *C. elegans*

791   genome (wormbase release WS285) using bwa-mem (version 0.7.17)[72]. Reads with

792   mapping quality (MAPQ) higher than 10 were extracted using Samtools[73]. ATAC-seq peaks

793   were called by first generating read depth-normalized coverage tracks with MACS2[74]

794   (version 2.7.1; settings: --nomodel –extsize 150 –shift -75 --keep-dup all –SPMR --

795   nolambda) and then running YAPC[71] (version 0.1) using bigwig tracks from both replicates

796   for each condition as input. CeSPT-2 ChIP-seq peaks were called using MACS2 (settings: -

797   -SPMR --gsize ce --keep-dup all --nomodel --broad) using the GFP ChIP-seq samples from

798   wild type animals as controls. The final SPT-2 peak set was defined by the strict

799   intersection of the broad peaks called on each replicate.

800   RNA-seq data were aligned on annotated transcripts (Wormbase release WS285; gene

801   types included: protein coding, lincRNAs and pseudogenes) using kallisto[75] (version 0.45.0)

802   to estimate gene expression (in TPM). Coverage profiles were obtained by aligning reads to

803   the genome using STAR[76] (version 2.7.1a).

804

Annotation of CeSPT-2 bound genes

806 A gene was considered a CeSPT-2 target if more than 50% of the length of its longest

807 annotated transcript was covered by a CeSPT-2 peak. The average CeSPT-2 coverage

808 over CeSPT-2 targets was calculated using coverageBed from the BEDTools suite[77]

809 (v.2.30.0). Coverage plots over gene models were produced using the DeepTools suite[78]

810 (version 3.5.1).

811

ATAC-seq

813 Animals of the indicated genotype (grown at 20°C) were bleached, and embryos allowed to

814 hatch overnight in M9 buffer. Approximately 12,000 L1 worms were seeded onto a 15cm

815 plates seeded with a thick lawn of HB101 bacteria. Gravid adult worms were collected 70h

816 post-seeding and washed three times in M9 buffer. To assess that worm synchronization

817 was equal between samples, 10µl of worm slurry was fixed in cold methanol overnight at -

818 20°C; the remaining slurry was frozen in 'popcorns'. The methanol-fixed worms were

819 stained with DAPI (final 1µg/ml) for 10 minutes, washes three times with PBS/0.1% Tween,

820 and rehydrated overnight at 4°C in PBS/0.1% Tween. Worms were then mounted on a slide

821 and inspected on a Leica SP8 UV microscope. ATAC-seq was performed as previously

822 described[71]. Frozen worms (3-4 frozen popcorns) were broken by grinding in a mortar and

823 pestle. The frozen powder was thawed in 10ml Egg buffer (25mM HEPES pH 7.3, 118mM

824 NaCl, 48mM KCl, 2mM $CaCl_2$, 2mM $MgCl_2$) and washed twice with that buffer by spinning 2

825 minutes at 1500g. After the second wash, the pellet was resuspended into 1.5ml of Egg

826 buffer containing 1mM DTT, protease inhibitors (Roche complete, EDTA free) and 0.025%

827 of Igepal CA-630. Samples were dounced 20 times in a 7ml stainless tissue grinder (VWR)

828 and then spun at 200g for 5min to pellet large debris. Supernatant containing nuclei was

829 transferred into a new tube and nuclei were counted using a haemocytometer. One million

830 nuclei were transferred to a new 1.5ml tube and spun at 1000g for 10 minutes, the

831 supernatant was removed, and the nuclei resuspended in 47.5µl of Tagmentation buffer

832 (containing 25µl of 2x Tagmentation buffer from Illumina and 22.5µl of water) before adding

833 2.5µl of Tn5 enzyme (Illumina Nextera kit) and incubated for 30 minutes at 37°C.

834 Tagmented DNA was then purified using MinElute column (Qiagen) and amplified 10 cycles

835 using the Nextera kit protocol. Amplified libraries were finally size selected using AMPure

836 beads to recover fragments between 150 and 500bp and sequenced.

837

Analysis of differentially accessible genes (ATAC-seq)

We used DiffBind[79] (version 3.8.0) to identify genes showing differential accessibility in the *spt-2*[KO-A] and the *spt-2*[HBM] strains compared to the wild type. For this analysis, we had to redefine gene coordinates to avoid overlaps, which would be otherwise merged in DiffBind. The boundaries of the longest transcript for each gene were trimmed to remove overlaps with neighbouring transcripts; if more than 50% of the length of the transcript was trimmed, the whole gene locus was removed from the analysis. Genes were defined as differentially accessible if the |LFC| > 0 and FDR < 0.05, and their enrichment evaluated at non-CeSPT-2 targets and at CeSPT-2 targets divided in 4 equally-sized groups based on their CeSPT-2 levels.

Collection of adult worms for total RNA extraction

Animals of the indicated genotype (grown at 20°C) were bleached, and embryos were allowed to hatch overnight in M9 buffer. Approximately 2000 L1 worms were seeded onto 10cm plates seeded with HB101 bacteria. Gravid adult worms were collected 70h post-seeding, washed three times in M9 buffer and the worm pellet was resuspended in 1mL Trizol (ThermoFisher, 15596026). This mixture was quickly thawed in a water bath at 37°C, followed by vortexing and freezing in liquid nitrogen; five freeze/thaw cycles were performed. Then, 200µl of chloroform were added, and the mixture was vortexed for 15 seconds and incubated at room temperature for 3 minutes. The mixture was spun down for 15 minutes at 15,000g in a refrigerated centrifuge (4°C). The upper aqueous phase was carefully moved to a new 1.5ml tube and RNA was retrieved by isopropanol precipitation. Briefly, 1µl of glycogen and 500µl of isopropanol was added and, after vortexing, the mixture was incubated overnight at -20°C. The next day, the mix was centrifuged for 15 minutes at 15,000g, 4°C and the supernatant removed. 1mL of 70% EtOH was added, and the tube was again centrifuged for 5 minutes at 15,000g, 4°C. After carefully removing the supernatant, the RNA pellet was allowed to dry at room temperature for a maximum of 5 minutes and then resuspended in 40µl DEPC-treated water (Invitrogen). The RNA quality was assessed on an Agilent Tapestation, using the RNA ScreenTape kit according to the manufacturer's instructions (Agilent, 5067-5576 and 5067-5577).

Poly(A) enrichment, library preparation and sequencing

Total RNA extracted from adult worms was treated with Turbo DNA-free kit (Invitrogen, AM1907) according to the manufacturer's protocol. RNA concentration was measured with

37

872   a Qubit instrument and 1μg of total RNA was used to make libraries. Poly(A) tail selection

873   was performed using NEBNext Poly(A) mRNA Magnetic Isolation Module (NEB, E7490S)

874   and libraries for next-generation sequencing were prepared using the NEBNext Ultra™ II

875   Directional RNA Library Prep kit with Sample Purification Beads (NEB, E7765S). Libraries

876   were indexed using NEBNext Multiplex Oligos for Illumina Index Primers Set 1 and 2

877   (E7335S and E7500S). Sequencing was performed on a NovaSeq instrument, 100bp

878   paired end sequencing.

879

880   **Differential gene expression**

881   We used DESeq2[80] (version 1.34.0) to identify genes differentially expressed in the *spt-2*[KO]

882   and the *spt-2*[HBM] strains compared to the wild type. Genes were defined as differentially

883   expressed if the |LFC| > 0 and p.adj < 0.001. Volcano plots were generated using the

884   EnhancedVolcano R package (available at

885   https://github.com/kevinblighe/EnhancedVolcano). GO-enrichment analysis of differentially

886   expressed genes was performed using clusterProfiler[81]. The overlap between genes

887   upregulated in *spt-2* and *hira-1* mutant[36] was tested using an hypergeometric test.

888

889   **RT-qPCR**

890   For the retro-transcription reaction, 1μl of 50μM random hexamers and 1μl of 10μM dNTPs

891   were added to 200-500ng of RNA in a 10μl volume reaction. The reactions were heated for

892   5 minutes at 65°C to denature secondary structures and allow random primer annealing.

893   Then, 4μl of 5x First strand buffer, 2μl of 0.1M DTT, 1μl of RNaseOUT and 1μl of

894   SuperScript RT III were added. This mix was incubated on a thermocycler with the following

895   program: 10 minutes at 25°C, 1 hour at 50°C and 15 min at 70°C. Before proceeding with

896   the qPCR reaction, the mix was diluted 1:5 with Sigma water.

897   qPCR primer sequences (5' – 3') are:

898   GSA144 gfp_ex1_F: GTGAAGGTGATGCAACATACGG (from ref. [82])

899   GSA145 gfp_ex1/2junction_R: ACAAGTGTTGGCCATGGAAC (from ref. [82])

900   GSA146 cdc-42 F: CTGCTGGACAGGAAGATTACG (from ref. [82])

901   GSA147 cdc-42 R: CTCGGACATTCTCGAATGAAG (from ref. [82])

902   GSA213 R06C1.4 F1: GTGTACGATCGTGAAACCGG

903   GSA214 R06C1.4 R1: CGAAGGTTGCGTCCATTGAA

904   GSA215 Y57G11B.5 F1: GCTTGTAATGCCGAGACGAG

905   GSA216 Y57G11B.5 R1: TGGAACATTTCGAGACGGGA

906   GSA217 asp-1 F1: GATTCCAGCCATTCGTCGAC

907   GSA218 asp-1 R1: TGATCCGGTGTCAAGAACGA

908   GSA221 clec-66 F1: TGCCATGACTAAATTCGCCG

909   GSA222 clec-66 R1: ACGCTCTCTTCTGTTGGTCA

910   GSA223 F08B12.4 F1: GAAAAGCGTCTTGGAAGGGG

911   GSA224 F08B12.4 R1: TTACTGGTGGTTTTGCTCGC

912   GSA225 C14C6.5 F1: CTACGACAATGGCACCAACC

913   GSA227 C14C6.5 R1: TTCATTCCTGGGCAGTCACT

914   GSA227 skr-10 F1: TGAGAGAGCTGCAAAGGAGA

915   GSA228 skr-10 R1: TGGAAGTCGATGGTTCAGCT

916   GSA350 H3.3-SNAP F2: CCTGGCTCAACGCCTACTTT (from ref. [59])

917   GSA351 H3.3-SNAP R2: GGTAGCTGATGACCTCTCCG (from ref. [59])

918   GSA352 H3.3-SNAP F3: TCGGAGAGGTCATCAGCTAC

919   GSA353 H3.3-SNAP R3: CAGAATGGGCACGGGATTTC

920

921   **Human cell culture**

922   All cells were kept at 37°C under humidified conditions with 5% CO_2. Parental U-2-OS cells

923   were grown in DMEM (Life Technologies) supplemented with 100 U/ml penicillin, 100µg/ml

924   streptomycin, 1% L-glutamate (Invitrogen), and 10% foetal bovine serum. U-2-OS SNAP-

925   H3.3 cells were described before[49] and were grown in the medium described above

926   supplemented with 100µg/ml G418 (Formedium, G4181S). To generate stable U-2-OS Flp-

927   In Trex cell lines, hygromycin was used to select for the integration of GFP-SPT2 constructs

928   at the Flp-In recombination sites. U-2-OS Flp-In Trex cells expressing GFP-tagged SPT2

929   were grown in the medium described above supplemented with 100µg/ml hygromycin and

930   10µg/ml blasticidin. Expression of GFP–SPT2 was induced by addition of 1 µg/ml of

931   tetracycline for 24 hours. All cell lines tested negative for mycoplasma contamination.

932

933   **siRNA transfection**

934   Twenty-four hours prior to transfection, 80,000 U-2-OS cells were seeded per 6-well dish.

935   siRNA transfection was performed with RNAiMax reagent (Invitrogen) according to the

936   manufacturer's protocol and all siRNAs were used to a final concentration of 50nM. Cells

937   were harvested 48 hours post-transfection. siRNA sequences (5' – 3') are the following:

938   Universal siRNA control (Sigma, SIC001)

939   siSPT2#1: GACCTATGACCGCAGAAGA

940   siSPT2#2: GTTACAATGGGATTCCTAT

941   siSPT2#3: GAGAATTCCTTGAACGAAA

942   siHIRA#1 GAAGGACUCUCGUCUCAUG (from ref. [83])

943

Soluble/chromatin fractionation

945   To analyse soluble and chromatin-bound proteins by western blotting, cells were washed in

946   cold PBS, scraped, and centrifuged at 1,500g for 10 minutes at 4°C. The pellet was

947   incubated on ice for 10 minutes in CSK buffer (10mM PIPES pH 7, 100mM NaCl, 300mM

948   sucrose, 3mM $MgCl_2$)/0.5% Triton X-100, supplemented with Roche Complete Protease

949   Inhibitor cocktail and PhosSTOP Roche phosphatase inhibitors, followed by 5 minutes

950   centrifugation at 1,500g, 4°C (Soluble fraction). The pellet was washed with CSK/0.5%

951   Triton, prior to resuspending in 1xLDS buffer supplemented with 10mM $MgCl_2$, 150mM DTT

952   and 250 units of Pierce Universal Nuclease (ThermoFisher, 88702), and incubated at 37°C

953   shaking for 1 hour (Chromatin fraction).

954

RNA extraction from human cells

956   RNA was extracted from U-2-OS cells according to the Qiagen RNeasy Mini Extraction kit.

957   DNaseI digestion was performed on columns using the Qiagen RNase-Free DNase Set.

958

Fluorescence analysis of human GFP-SPT2

960   To analyse GFP-SPT2 intensity on chromatin, U-2-OS Flp-In cells grown in 96-well plates

961   (Greiner) were treated with 1µg/ml tetracycline for 24 hours to induce expression of GFP-

962   tagged SPT2. Cells were then either directly fixed with 4% paraformaldehyde (10 minutes

963   at room temperature), or pre-extracted for 5 minutes on ice with CSK/0.5% Triton buffer

964   (supplemented with Roche Complete Protease inhibitor and PhosSTOP Phosphatase

965   inhibitors) to remove soluble proteins, prior to fixation for 10 minutes with 4%

966   paraformaldehyde at room temperature. DNA was stained with DAPI, and images were

967   acquired using a Perkin Elmer Operetta high-content automated microscope (equipped with

968   a 20X dry objective) and analysed using the Perkin Elmer Columbus software.

969

Western blotting and antibodies

971   Primary antibodies: human SPT2 (in-house produced, DA010), GAPDH (Cell Signalling,

972   clone 14C10, 2118S), GFP (Abcam, ab290), RPB1 (Cell Signalling, clone D8L4Y, 14958S),

973   HIRA (Active Motif, 39457), His_6 (Abcam, ab18184), H3 (Abcam, ab1791). Secondary

974 IRDye LI-COR antibodies were used. Images were acquired using an Odyssey CLx LI-COR

975 scanner.

976

977 **Human SPT2 antibody production**

978 Polyclonal SPT2 antibodies were raised in sheep by the MRC PPU Reagents and Services

979 Unit (University of Dundee) and purified against the SPT2 antigen aa. 385-685 (after

980 depleting antibodies recognizing the epitope tags). Sheep DA010, 3rd bleed, was used in

981 this study. Sheep were immunised with the antigens followed by four further injections 28

982 days apart. Bleeds were performed seven days after each injection.

983

984 **SNAP-tag labelling**

985 For labeling newly synthesized SNAP-tagged histones in U-2-OS cells stably expressing

986 H3.3-SNAP, pre-existing SNAP-tagged histones were first quenched by incubating cells

987 with 10 µM of the non-fluorescent SNAP reagent (SNAP-cell Block, New England Biolabs)

988 for 30 min at 37°C followed by a 30 min wash in fresh medium and a 2-hour chase.

989 The SNAP-tagged histones neosynthesized during the chase time were then pulse-labelled

990 by incubating cells with 2 µM of the red-fluorescent SNAP reagent SNAP-cell TMR star

991 (New England Biolabs) for 15 min at 37°C, followed by a 45 min wash in fresh medium.

992 Cells were then directly fixed in 2% paraformaldehyde or pre-extracted before fixation in

993 CSK buffer containing 0.5% Triton X-100. Samples were observed with a Leica DMI6000

994 epifluorescence microscope using a Plan-Apochromat 40x/1.3 oil objective. Images were

995 captured using a CCD camera (Photometrics) and Metamorph software. Fiji software was

996 used for image analyses using custom macros. Nuclei were delineated based on DAPI

997 staining.

998

999 **Statistical analysis**

1000 The difference of variance between two populations was measured using Prism 9 software,

1001 and a Welch's correction was applied when the variances were not equal. p values are

1002 provided and defined in the legend of the figure. The multiple comparisons in Fig. 5d and e

1003 were performed with One-way ANOVA test with Bonferroni's correction. The overlap

1004 between genes upregulate in *spt-2* and *hira-1* mutant worms (Fig. 5g) was performed using

1005 a hypergeometric test.

1006

1007 ***C. elegans* strains**

41

Genotype	Strain name	Source
WT N2		CGC
spt-2(syb1268) IV	JRG30	This work, from SunyBiotech
spt-2(syb1269) IV	JRG31	This work, from SunyBiotech
spt-2(syb2412[M627A]*) IV*	JRG48	This work, from SunyBiotech
spt-2(syb1735[mAID-gfp::spt-2(wt)]) IV	JRG44	This work, from SunyBiotech
spt-2(syb2435[mAID-gfp::spt-2(M627A)) IV	JRG45	This work, from SunyBiotech
spt-2(syb2412,syb4133[A627M]) IV	PHX4133	This work, from SunyBiotech
mjIs31 II	SX461	From ref. [42]
mjIs31 II; hrde-1(tm1200) III	SX3448	From ref. [82]
mjIs31 II; spt-2(syb1268) IV	JRG49	This work
mjIs31 II; spt-2(syb1269) IV	JRG50	This work
mjIs31 II; spt-2(syb2412[M627A]*) IV* sibling 1	JRG51	This work
mjIs31 II; spt-2(syb2412[M627A]*) IV* sibling 2	JRG52	This work

1008

1009 **Plasmids**

Plasmid name	DSTT Reference
2xFlag-SUMO-CeSPT-2-His$_6$ full-length	DU70523
2xFlag-SUMO-CeSPT-2-His$_6$ full-length M627A	DU70525
2xFlag-SUMO-HsSPT2-His$_6$ full-length	DU70522
His$_{14}$-SUMO-CeSPT-2 HBD (aa. 551-662)	DU70520
His$_{14}$-SUMO-CeSPT-2 HBD (aa. 551-662) M627A	DU70521
His$_{14}$-SUMO-HsSPT-2 HBD (aa. 571-685)	DU70518
His$_{14}$-SUMO-HsSPT-2 HBD (aa. 571-685) M641A	DU70519
pcDNA5-FRT/TO-GFP	DU13156
pcDNA5-FRT/TO-GFP-SPT2	DU63205
pcDNA5-FRT/TO-SPT2-GFP	DU63486

pcDNA5-FRT/TO-GFP-SPT2 1-570	DU63519
pcDNA5-FRT/TO-GFP-SPT2 571-end	DU63517
L4440	DU70356
L4440-*gfp*	From ref. [82]
L4440-*hira-1*	Source Bioscience

1010
1011
1012

References

1. Luger, K., Mader, A.W., Richmond, R.K., Sargent, D.F. & Richmond, T.J. Crystal structure of the nucleosome core particle at 2.8 A resolution. *Nature* **389**, 251-60 (1997).

2. Venkatesh, S. & Workman, J.L. Histone exchange, chromatin structure and the regulation of transcription. *Nat Rev Mol Cell Biol* **16**, 178-89 (2015).

3. Ferrand, J., Plessier, A. & Polo, S.E. Control of the chromatin response to DNA damage: Histone proteins pull the strings. *Semin Cell Dev Biol* **113**, 75-87 (2021).

4. Stewart-Morgan, K.R., Petryk, N. & Groth, A. Chromatin replication and epigenetic cell memory. *Nat Cell Biol* **22**, 361-371 (2020).

5. Hammond, C.M., Stromme, C.B., Huang, H., Patel, D.J. & Groth, A. Histone chaperone networks shaping chromatin function. *Nat Rev Mol Cell Biol* **18**, 141-158 (2017).

6. Pardal, A.J., Fernandes-Duarte, F. & Bowman, A.J. The histone chaperoning pathway: from ribosome to nucleosome. *Essays Biochem* **63**, 29-43 (2019).

7. Martire, S. & Banaszynski, L.A. The roles of histone variants in fine-tuning chromatin organization and function. *Nat Rev Mol Cell Biol* **21**, 522-541 (2020).

8. Formosa, T. & Winston, F. The role of FACT in managing chromatin: disruption, assembly, or repair? *Nucleic Acids Res* **48**, 11929-11941 (2020).

9. Kujirai, T. & Kurumizaka, H. Transcription through the nucleosome. *Curr Opin Struct Biol* **61**, 42-49 (2020).

10. Teves, S.S., Weber, C.M. & Henikoff, S. Transcribing through the nucleosome. *Trends Biochem Sci* **39**, 577-86 (2014).

11. Kujirai, T. et al. Structural basis of the nucleosome transition during RNA polymerase II passage. *Science* **362**, 595-598 (2018).

12. Hall, M.A. et al. High-resolution dynamic mapping of histone-DNA interactions in a nucleosome. *Nat Struct Mol Biol* **16**, 124-9 (2009).

13. Farnung, L., Ochmann, M., Engeholm, M. & Cramer, P. Structural basis of nucleosome transcription mediated by Chd1 and FACT. *Nat Struct Mol Biol* **28**, 382-387 (2021).

14. Farnung, L., Vos, S.M. & Cramer, P. Structure of transcribing RNA polymerase II-nucleosome complex. *Nat Commun* **9**, 5432 (2018).

15. Liu, Y. et al. FACT caught in the act of manipulating the nucleosome. *Nature* **577**, 426-431 (2020).

16. Evrin, C. et al. Spt5 histone binding activity preserves chromatin during transcription by RNA polymerase II. *EMBO J* **41**, e109783 (2022).

17. Jeronimo, C., Poitras, C. & Robert, F. Histone Recycling by FACT and Spt6 during Transcription Prevents the Scrambling of Histone Modifications. *Cell Rep* **28**, 1206-1218 e8 (2019).

18. Torne, J. et al. Two HIRA-dependent pathways mediate H3.3 de novo deposition and recycling during transcription. *Nat Struct Mol Biol* **27**, 1057-1068 (2020).

19. Belotserkovskaya, R. et al. FACT facilitates transcription-dependent nucleosome alteration. *Science* **301**, 1090-3 (2003).

20. Jamai, A., Puglisi, A. & Strubin, M. Histone chaperone spt16 promotes redeposition of the original h3-h4 histones evicted by elongating RNA polymerase. *Mol Cell* **35**, 377-83 (2009).

21. Goldberg, A.D. et al. Distinct factors control histone variant H3.3 localization at specific genomic regions. *Cell* **140**, 678-91 (2010).

22. Ray-Gallet, D. et al. Dynamics of histone H3 deposition in vivo reveal a nucleosome gap-filling mechanism for H3.3 to maintain chromatin integrity. *Mol Cell* **44**, 928-41 (2011).

23. Schwartz, B.E. & Ahmad, K. Transcriptional activation triggers deposition and removal of the histone variant H3.3. *Genes Dev* **19**, 804-14 (2005).

24. Tagami, H., Ray-Gallet, D., Almouzni, G. & Nakatani, Y. Histone H3.1 and H3.3 complexes mediate nucleosome assembly pathways dependent or independent of DNA synthesis. *Cell* **116**, 51-61 (2004).

25. Chen, S. et al. Structure-function studies of histone H3/H4 tetramer maintenance during transcription by chaperone Spt2. *Genes Dev* **29**, 1326-40 (2015).

26. Nourani, A., Robert, F. & Winston, F. Evidence that Spt2/Sin1, an HMG-like factor, plays roles in transcription elongation, chromatin structure, and genome stability in Saccharomyces cerevisiae. *Mol Cell Biol* **26**, 1496-509 (2006).

27. Winston, F., Chaleff, D.T., Valent, B. & Fink, G.R. Mutations affecting Ty-mediated expression of the HIS4 gene of Saccharomyces cerevisiae. *Genetics* **107**, 179-97 (1984).

28. Sternberg, P.W., Stern, M.J., Clark, I. & Herskowitz, I. Activation of the yeast HO gene by release from multiple negative controls. *Cell* **48**, 567-77 (1987).

29. Bhat, W., Boutin, G., Rufiange, A. & Nourani, A. Casein kinase 2 associates with the yeast chromatin reassembly factor Spt2/Sin1 to regulate its function in the repression of spurious transcription. *Mol Cell Biol* **33**, 4198-211 (2013).

30. Novoseler, M., Hershkovits, G. & Katcoff, D.J. Functional domains of the yeast chromatin protein Sin1p/Spt2p can bind four-way junction and crossing DNA structures. *J Biol Chem* **280**, 5169-77 (2005).

31. Zlatanova, J. & van Holde, K. Binding to four-way junction DNA: a common property of architectural proteins? *FASEB J* **12**, 421-31 (1998).

32. Osakabe, A. et al. Vertebrate Spt2 is a novel nucleolar histone chaperone that assists in ribosomal DNA transcription. *J Cell Sci* **126**, 1323-32 (2013).

33. Ahringer, J. & Gasser, S.M. Repressive Chromatin in Caenorhabditis elegans: Establishment, Composition, and Function. *Genetics* **208**, 491-511 (2018).

34. Zeller, P. et al. Histone H3K9 methylation is dispensable for Caenorhabditis elegans development but suppresses RNA:DNA hybrid-associated repeat instability. *Nat Genet* **48**, 1385-1395 (2016).

35. Nakano, S., Stillman, B. & Horvitz, H.R. Replication-coupled chromatin assembly generates a neuronal bilateral asymmetry in C. elegans. *Cell* **147**, 1525-36 (2011).

36. Burkhart, K.B., Sando, S.R., Corrionero, A. & Horvitz, H.R. H3.3 Nucleosome Assembly Mutants Display a Late-Onset Maternal Effect. *Curr Biol* **30**, 2343-2352 e3 (2020).

1099   37.   Delaney, K., Mailler, J., Wenda, J.M., Gabus, C. & Steiner, F.A. Differential
1100   Expression of Histone H3.3 Genes and Their Role in Modulating Temperature Stress
1101   Response in Caenorhabditis elegans. *Genetics* **209**, 551-565 (2018).
1102   38.   Kolundzic, E. et al. FACT Sets a Barrier for Cell Fate Reprogramming in
1103   Caenorhabditis elegans and Human Cells. *Dev Cell* **46**, 611-626 e12 (2018).
1104   39.   Gartner, A., Boag, P.R. & Blackwell, T.K. Germline survival and apoptosis.
1105   *WormBook*, 1-20 (2008).
1106   40.   McMurchy, A.N. et al. A team of heterochromatin factors collaborates with small
1107   RNA pathways to combat repetitive elements and germline stress. *Elife* **6**(2017).
1108   41.   Spracklin, G. et al. The RNAi Inheritance Machinery of Caenorhabditis elegans.
1109   *Genetics* **206**, 1403-1416 (2017).
1110   42.   Ashe, A. et al. piRNAs can trigger a multigenerational epigenetic memory in the
1111   germline of C. elegans. *Cell* **150**, 88-99 (2012).
1112   43.   Buckley, B.A. et al. A nuclear Argonaute promotes multigenerational epigenetic
1113   inheritance and germline immortality. *Nature* **489**, 447-51 (2012).
1114   44.   Kalinava, N. et al. C. elegans Heterochromatin Factor SET-32 Plays an Essential
1115   Role in Transgenerational Establishment of Nuclear RNAi-Mediated Epigenetic
1116   Silencing. *Cell Rep* **25**, 2273-2284 e3 (2018).
1117   45.   Schwartz-Orbach, L. et al. Caenorhabditis elegans nuclear RNAi factor SET-32
1118   deposits the transgenerational histone modification, H3K23me3. *Elife* **9**(2020).
1119   46.   Burkhart, K.B. et al. A pre-mRNA-associating factor links endogenous siRNAs to
1120   chromatin regulation. *PLoS Genet* **7**, e1002249 (2011).
1121   47.   Burton, N.O., Burkhart, K.B. & Kennedy, S. Nuclear RNAi maintains heritable gene
1122   silencing in Caenorhabditis elegans. *Proc Natl Acad Sci U S A* **108**, 19683-8 (2011).
1123   48.   Woodhouse, R.M. & Ashe, A. How do histone modifications contribute to
1124   transgenerational epigenetic inheritance in C. elegans? *Biochem Soc Trans* **48**,
1125   1019-1034 (2020).
1126   49.   Dunleavy, E.M., Almouzni, G. & Karpen, G.H. H3.3 is deposited at centromeres in S
1127   phase as a placeholder for newly assembled CENP-A in G(1) phase. *Nucleus* **2**,
1128   146-57 (2011).
1129   50.   Segura-Bayona, S. et al. Tousled-Like Kinases Suppress Innate Immune Signaling
1130   Triggered by Alternative Lengthening of Telomeres. *Cell Rep* **32**, 107983 (2020).
1131   51.   Lev, I., Gingold, H. & Rechavi, O. H3K9me3 is required for inheritance of small
1132   RNAs that target a unique subset of newly evolved genes. *Elife* **8**(2019).
1133   52.   Woodhouse, R.M. et al. Chromatin Modifiers SET-25 and SET-32 Are Required for
1134   Establishment but Not Long-Term Maintenance of Transgenerational Epigenetic
1135   Inheritance. *Cell Rep* **25**, 2259-2272 e5 (2018).
1136   53.   Kruger, W. & Herskowitz, I. A negative regulator of HO transcription, SIN1 (SPT2), is
1137   a nonspecific DNA-binding protein related to HMG1. *Mol Cell Biol* **11**, 4135-46
1138   (1991).
1139   54.   Thapar, R. Structure-specific nucleic acid recognition by L-motifs and their diverse
1140   roles in expression and regulation of the genome. *Biochim Biophys Acta* **1849**, 677-
1141   87 (2015).

1142   55.   Deal, R.B., Henikoff, J.G. & Henikoff, S. Genome-wide kinetics of nucleosome
1143   turnover determined by metabolic labeling of histones. *Science* **328**, 1161-4 (2010).
1144   56.   Jamai, A., Imoberdorf, R.M. & Strubin, M. Continuous histone H2B and transcription-
1145   dependent histone H3 exchange in yeast cells outside of replication. *Mol Cell* **25**,
1146   345-55 (2007).
1147   57.   Dion, M.F. et al. Dynamics of replication-independent histone turnover in budding
1148   yeast. *Science* **315**, 1405-8 (2007).
1149   58.   Rufiange, A., Jacques, P.E., Bhat, W., Robert, F. & Nourani, A. Genome-wide
1150   replication-independent histone H3 exchange occurs predominantly at promoters
1151   and implicates H3 K56 acetylation and Asf1. *Mol Cell* **27**, 393-405 (2007).
1152   59.   Huang, H. et al. A unique binding mode enables MCM2 to chaperone histones H3-
1153   H4 at replication forks. *Nat Struct Mol Biol* **22**, 618-26 (2015).
1154   60.   Hammond, C.M. et al. DNAJC9 integrates heat shock molecular chaperones into the
1155   histone chaperone network. *Mol Cell* **81**, 2533-2548 e9 (2021).
1156
1157
1158
1159